Electronic Supplementary Material (ESI) for Chemical Science
This journal is © The Royal Society of Chemistry 2013

Direct Observation of a Cationic Ruthenium Complex for Ethylene Insertion Polymerization

Miguel Angel Camacho-Fernandez, Max Yen, Joseph Ziller, and Zhibin Guan *

Department of Chemisty, 1102 Natural Sciences 2, University of California, Irvine, California 92697-2025, United States

Supporting Information

Table of Contents

General. All organic synthesis and organometallic complexations were conducted under inert atmosphere by using standard Schlenk, vacuum, or glove box (N_2) techniques. Ethanol was degassed with N_2 prior to use. $[H(Et_2O)_2]^+$ $[BArF]^-$ (where Ar'= 3,5-$(CF_3)_2C_6H_3$)) was synthesized following Brookhart's procedure.[1]

^{1}H NMR, ^{13}C-NMR, NOE, and 2D-NMR spectra were recorded on a 500 MHz Bruker Avance GN-500, CRYO-500, or a Bruker Avance 600 MHz (for some insertion studies) spectrometer. All NMR chemical shifts are reported as δ in parts per million (ppm). ^{1}H and ^{13}C NMR spectra are relative to residual solvent. Coupling constants are reported in Hz. Electrospray Ionization Mass Spectrometric analyses (ESI-MS) were obtained on a Waters Micromass LCT ESI-MS. ESI-MS spectra analysis and isotope pattern simulations were carried out with MassLynx Mass Spectrometry software. Elemental analysis was performed by Atlantic Microlab, Inc.

All reagents were used as received from commercial suppliers unless otherwise noted. Anhydrous solvents were passed through a column of activated alumina (type A2, size 12x32, Purify) under argon pressure. Deuterated solvents were purchased from Cambridge Isotope Laboratories and were placed over activated 4Å molecular sieves. CD_2Cl_2 was dried over CaH_2 and distilled. Ultrahigh pure grade ethylene gas was purchased from Praxair and used without further purification.

Polyethylene molecular weight (Mw and Mn) was determined by High Temperature Gel Permeation Chromatography (HT-GPC) with polystyrene standards. Branching was determined by ^{1}H-NMR and expressed as the number of Me's per 1000 carbons.[2]

General procedure for ethylene polymerization. A 600 mL autoclave was heated under high vacuum to 120 °C for two hours then twice purged with ethylene and cooled to 0ºC. Two

Schlenk flasks of 50 and 100 mL respectively were kept in an oven overnight and introduced in the glove box. 100 mL of dry methylene chloride (DCM) solvent was measured. 10 mL of the solvent were used to dissolve the desired amount of complex **3** in the 50 mL flask. Another 10 mL were loaded into a syringe for later rising of the flask. The left 80 ml solution (DCM) was loaded with the desired amount of cocatalyst (1.0M solution of $AlMe_2Cl$ in Hexanes). The cocatalyst solution was then transferred into the reactor through cannula under inert atmosphere. The reactor was then filled with ethylene at 200 psi for 10 minutes. Solution of complex **3** was introduced through cannula under inert atmosphere and the flask was rinsed with the previously loaded syringe. Parr reactor was closed and pressurized and heated up to the desire values. Polymerization was quenched with a methanol-acidic solution (100 mL). Polyethylene was filtrated and washed with MeOH and acetone. Polyethylene was dried under high vacuum overnight.

Polymerizations with complex 4 (($[H(Et_2O)_2]^+$ $[BAr'_4]^-$) as activator). A 600 mL autoclave was heated under high vacuum to 120 °C for two hours then twice purged with ethylene and cooled to 0 ºC. A Schlenk flask (100 ml) was dried overnight and introduced in a glove box. The desired amount of complex **4** is measured from a stock solution in DCM and loaded into the 100 mL flask. The flask containing complex **4** is filled with DCM to complete a total volume of 100 mL. A 15 mL vial, previously dried overnight, is used to weight 1 equivalent of ($[H(Et_2O)_2]^+$ $[BAr'_4]^-$) and dissolved in a small amount of DCM (10 mL) and loaded in a 12 mL syringe. The solution containing complex **4** is taken out of the glove box and flushed with ethylene at -78 °C for 15 minutes. ($[H(Et_2O)_2]^+$ $[BAr'_4]^-$) solution in the above mention 12 mL syringe is added, this will make complex **5** in situ. Solution containing complex **5** is then loaded in the Parr reactor through cannula under ethylene atmosphere. Reactor is closed, pressurized with ethylene to the desired pressure, and heated up to the polymerization temperature. Polymerization is stopped by the addition of methanol (200ml). Polyethylene is purified by centrifuging at 8000 rpm for 10 minutes and dried overnight under high vacuum.

Molecular Modeling for Complexes 5A and 5B. All initial geometries were started from crystal data from complex **4** and replacing one methyl for ethylene. The computational softwareTurbomole[3] was used for all geometry optimizations and single point calculations. All calculations were run using density functional theory (DFT), with def2-SV(P) basis set for all the atoms. TPSS basis set for all atoms was used for single point calculations. The functional used was PBE for all calculations. Complex **5A** is more stable by 1 Kcal/mol at 298 K.

Complex RuCl$_2$(Ph(CH$_3$)$_3$SCH$_3$) (3): Synthesis and Characterization

Scheme S1

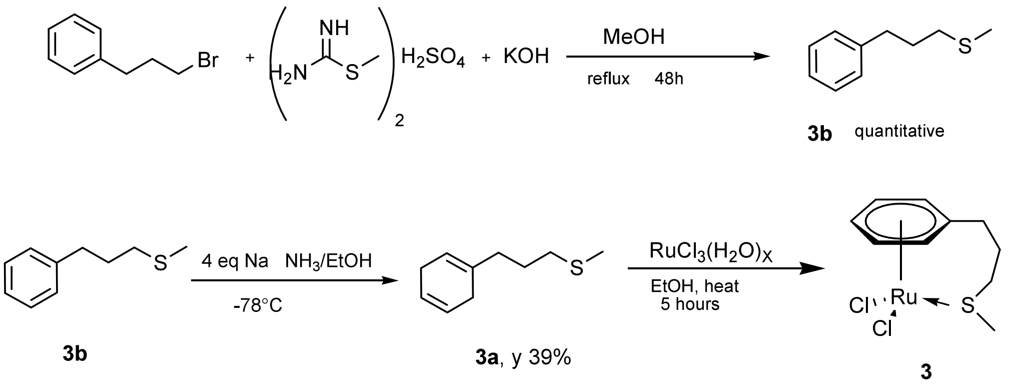

Synthesis of methyl(3-phenylpropyl)sulfide (3b). Similar to previously reported procedure.[4] 5.0336 g of 2-methyl thiopseudourea sulfate (0.018 mol, 1.8 eq) and 3.92770g (0.07 mol, 7 eq) of potassium hydroxide were dissolved in MeOH (50 mL), in a 100 mL round bottom flask. After 30 minutes of stirring, 2.0000g of 1-(3-bromopropyl)benzene (0.01 mol, 1 eq) was charged through a needle into the solution. The reaction mixture was heated at reflux for 2 days and monitored by TLC. Yellowish oil was obtained. Purification by high vacuum distillation afforded a colorless oil Yield: quantitative. ^{1}H NMR (500 MHz, $CDCl_3$): δ 7.21 (m, 2H), 7.12 (m, 3H), 2.65 (t, *J* = 7.5 Hz, 2H), 2.44 (t, *J* = 7.0 Hz, 2H), 2.03 (s, 2H), 2.22 (s, 3H), 1.85 (tt, *J* = 7.0, 7.5 Hz, 2H).

Synthesis of (3-(cyclohexa-1,4-dienyl)propyl)(methyl)sulfide (3a). Birch Reduction.[5] A two neck 500 mL round bottom flask was flame dried, cooled down in a dry ice/acetone bath (-78 °C) which was kept all the time. 60 mL of degassed ethanol were added and 2.3420 g (0.014 mol, 1 eq) of **3a** was added. Gaseous NH_3 (~240 mL) was liquefied into the flask with the help of dry ice/acetone mixture in a cold finger apparatus, and stirred for 10 minutes. Metal Sodium 1.5100 g (0.070 mol, 5 eq) was added portion wise. A 500 mL saturated solution of Ammonium Chloride (NH_4Cl) is added to the reaction flask. Product was isolated by repeated extractions with Ether (3 x 500 mL) and drying of the organic phase over Magnesium Sulfate. High vacuum distillation afforded a colorless oil. Yield: 0.6408g, 39%. ^{1}H NMR (500 MHz, $CDCl_3$): δ 5.70 (b, 2H), 5.44 (b, 1H), 2.68 (m, 2H), 2.59 (m, 2H), 2.49 (t, *J* = 6.5 Hz, 2H), 2.10 (s, 3H), 2.07 (t, *J* = 7.5 Hz, 2H), 1.85 (tt, *J* = 6.5, 7.5 Hz, 2H). ^{13}C NMR (500 MHz, $CDCl_3$): δ 134.3, 124.5, 124.4, 119.1, 36.6, 36.2, 34.0, 29.0, 26.9, 15.7.

Synthesis of [Ru(η^6- $Ph(CH_2)_3S(CH_3)_2Cl_2$] (3). 0.6408 g (0.0038 mol, 2 eq) of **3a** were added to degassed ethanol (10 mL) and stirred for 10 minutes. 0.4968 g (0.0019 mol, 1 eq) of $RuCl_3(H_2O)_x$ were added to the solution (calculations with x=3). The mixture was heated under reflux for 5 hours. The solution was left to reach room temperature and filtered to obtain an orange powder. The solid was washed with ether and hexanes under filtration and dried *in vacuo*. Red crystals suitable for analysis were obtained at 4°C from a solution in DCM/hexanes by slow diffusion. Yield: 0.5635 g, 87%. ^{1}H NMR (500 MHz, CD_2Cl_2, 298K): δ 6.03 (dd, 5.5, 5.5 Hz, 1H,), 5.00-5.40 (b, 2H), 5.20 (d, 5.5 Hz, 2H), 3.00-2.20 (b, 6H), 2.18 (s, 3H). ^{1}H NMR (500 MHz, CD_2Cl_2, 323K): δ 6.02 (dd, 5.0 Hz, 1H), 5.68 (b, 2H), 5.20 (d, 5.0 Hz, 2H), 2.70 (b, 2H), 2.60 (b, 2H), 2.40 (b, 2H), 2.22 (s, 3H). ^{1}H NMR (500 MHz, CD_2Cl_2, 203K): δ 6.05 (dd, 5.5, 6.0 Hz, 1H), 5.76 (dd, 5.5, 6.0 Hz, 1H), 5.66 (dd, 5.5, 5.5 Hz, 1H), 5.21 (d, 5.5 Hz, 1H), 5.18 (d, 5.5 Hz, 1H), 2.72-2.37 (m, 5H), 2.28 (m, 1H), 2.15 (s, 3H). ^{13}C NMR (500 MHz, CD_2Cl_2, 298K): δ 91.2, 89.6, 34.9, 30.5, 24.4, 18.6, carbon signals corresponding to carbons "e" and "f" figure S1 are not seen due to slow inversion at 298K. ESI-MS (ESI+, CH_2Cl_2) *m/z* calcd for $C_{10}H_{14}Cl_2SRu$ $[M]^+$, 338.26; found $[M-Cl]^+$, 302.95. Elemental Analysis: Anal. Calcd for C10H14Cl2RuS: C, 35.51; H, 4.17; Cl, 20.96; Ru, 29.88; S, 9.48. Found: C, 35.74; H, 4.19; S, 9.82.

Variable Temperature NMR Studies of complex **3**

Room temperature NMR displays very broad lines, in order to characterize the complex by NMR low and high temperature experiments were carried out. From the NMR experiments we are able to show the presence of two enantiomers as depicted on Scheme S2.

Scheme S2

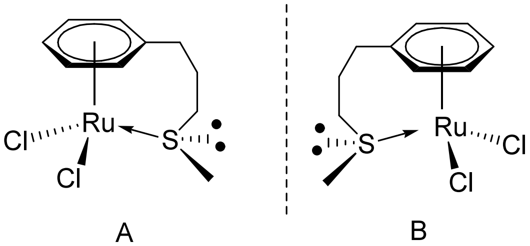

Figure S1 depicts the ^{1}H-NMR at 323 K in CD_2Cl_2, peaks are still broad but allow for protons assignment. Complex **3** displays poor solubility in most solvents, deuterated DCM is used to avoid peaks overlap with residual solvent.

Figure S2 is the ^{1}H-NMR of complex **3** at 203 K in CD_2Cl_2 at this temperature almost all protons can be assigned unambiguously except for the tethered arm protons due to signals overlap. Figure S3 depicts the comparison of complex **3** ^{1}H-NMR at different temperatures, at low temperatures both isomers are frozen. At higher temperatures the slow interconvertion between isomers broadens most proton signals except for protons "g" and "a" whose shifts are not affected by inversion at sulfur. NOESY allows assigning aromatic protons relatively with S-Me protons (figures S5 and S6).

Inversion Barrier was calculated from NMR by using the standard equation below. This insertion barrier has also being used for other sulfide coordinated organometallic complexes.[6]

$$k_c = \frac{\pi \Delta \nu}{\sqrt{2}} \cong 2.22\Delta\nu \quad rate\ constant\ at\ coalescence\ \Delta\nu(Hz)$$

$$\Delta G_c^{\neq} = RT\left[23.76 - \ln\left(\frac{k_c}{T_c}\right)\right] \quad \Delta G_c^{\neq}\ at\ coalescence\ T_c = 293\ K$$

Figure S3 displays the variable temperature NMR, coalescence of "f" peak was used (*$\Delta\nu$=50 Hz)*. Coalescence temperature was T_c=293 K. Inversion barrier at sulfur was determined to be 14.4±0.1 kcal·mol^{-1} in methylene chloride-d_2.

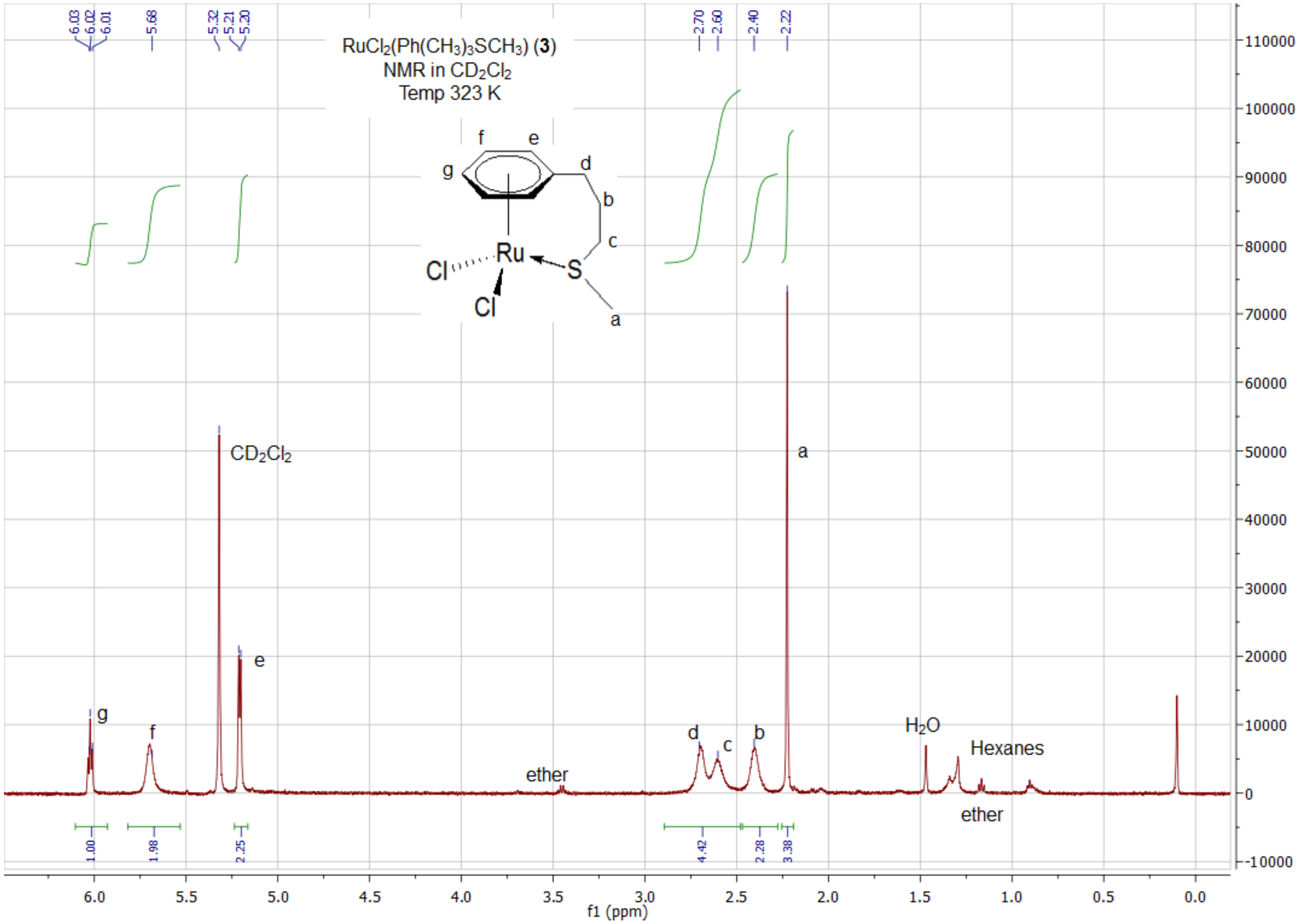

Figure S1. ^{1}H-NMR spectrum for complex **3** at 323 K in CD_2Cl_2.

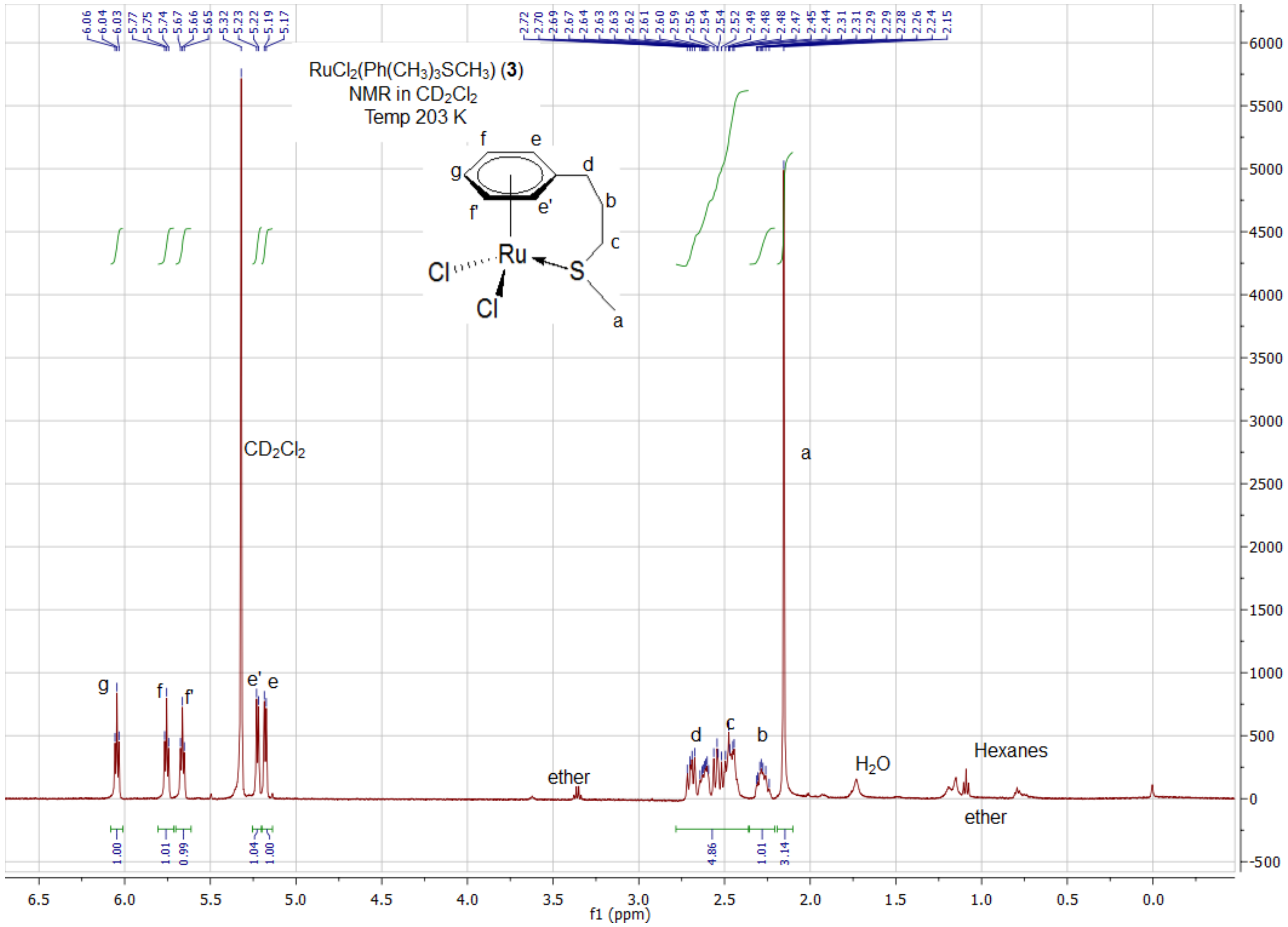

Figure S2. ^{1}H-NMR spectrum for complex **3** at 203 K in CD_2Cl_2.

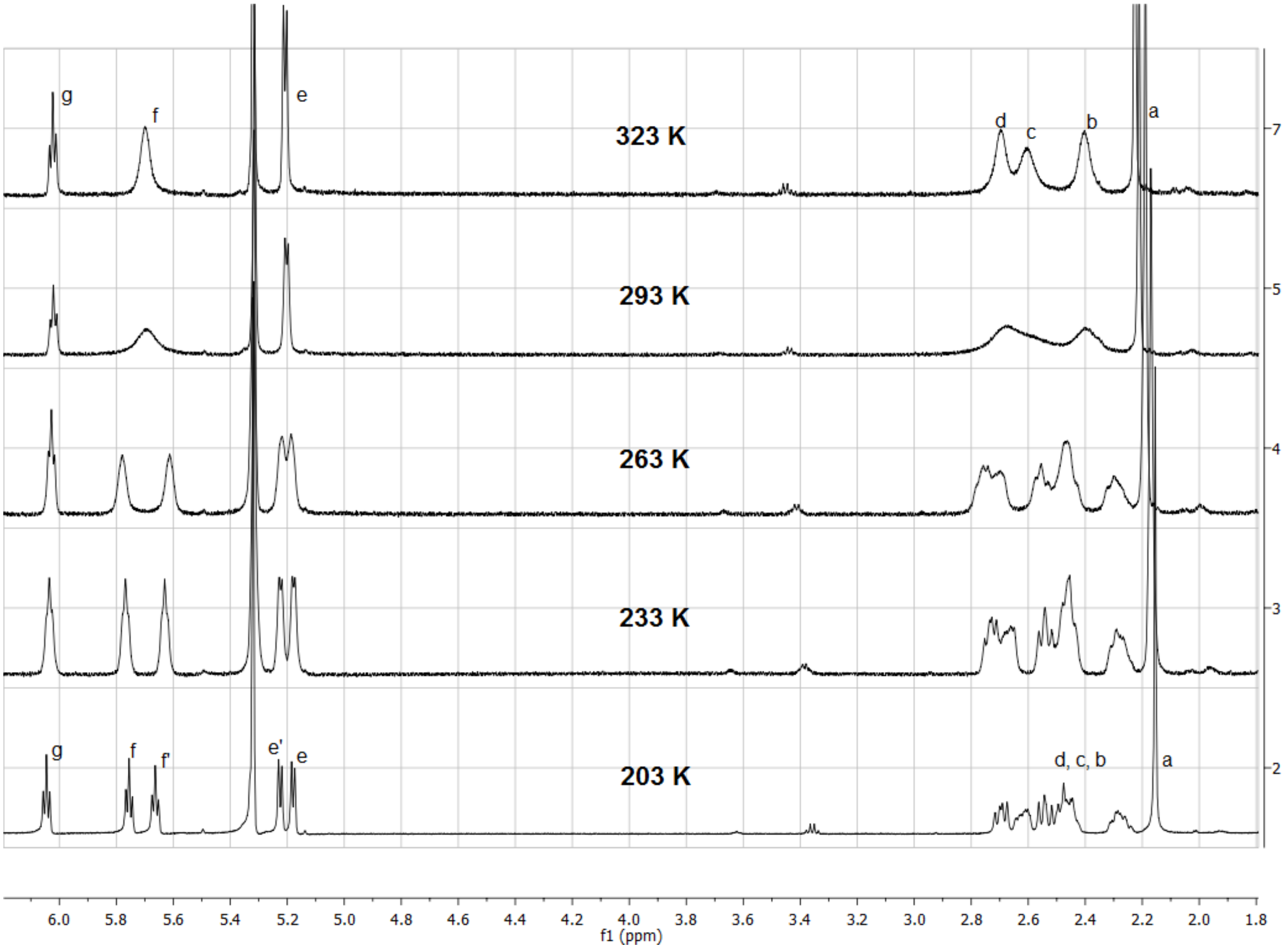

Figure S3. ^{1}H-NMR spectrum for complex **3** at different temperatures in CD_2Cl_2

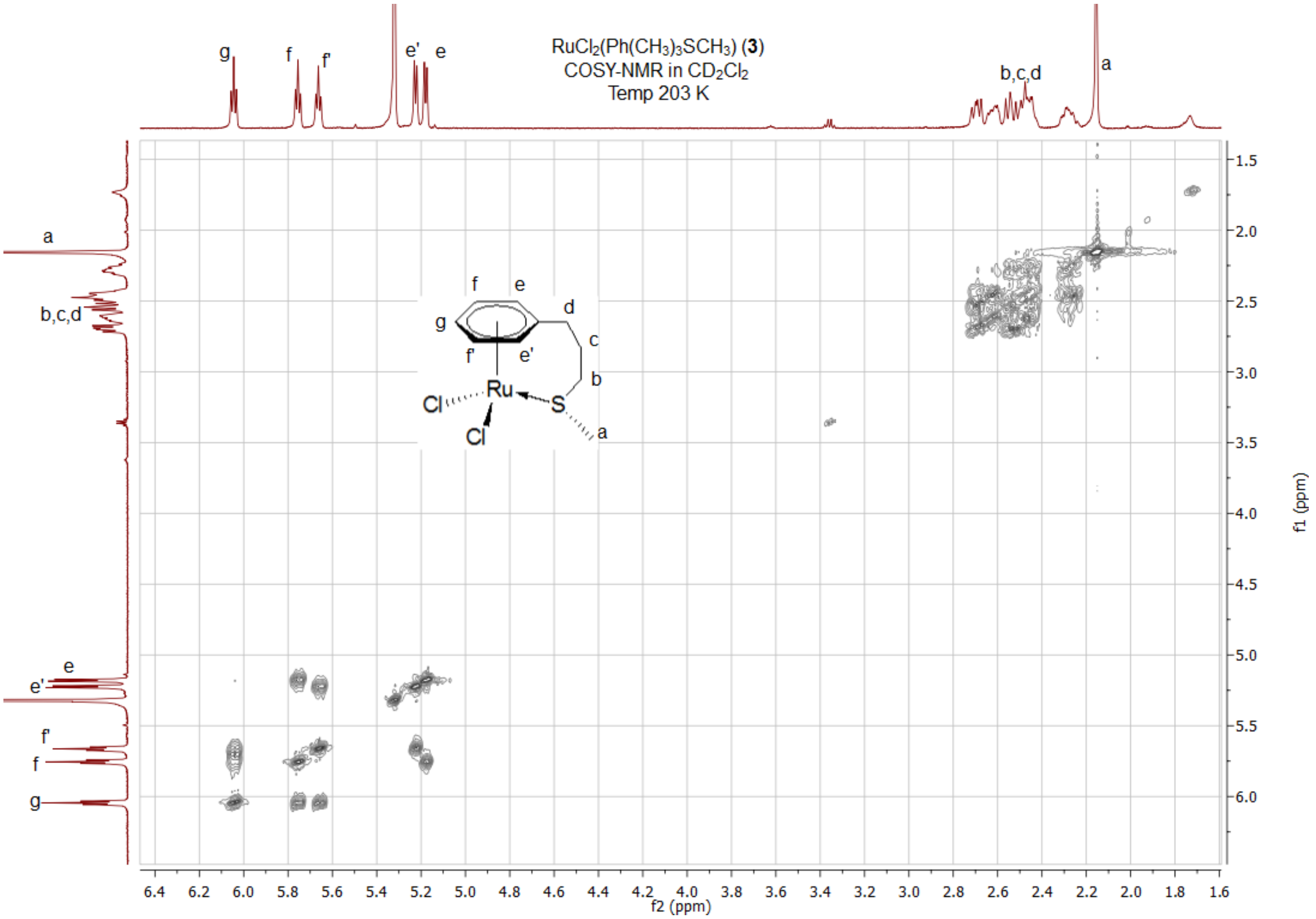

Figure S4. COSY-NMR spectrum for complex **3** at 203K in CD_2Cl_2.

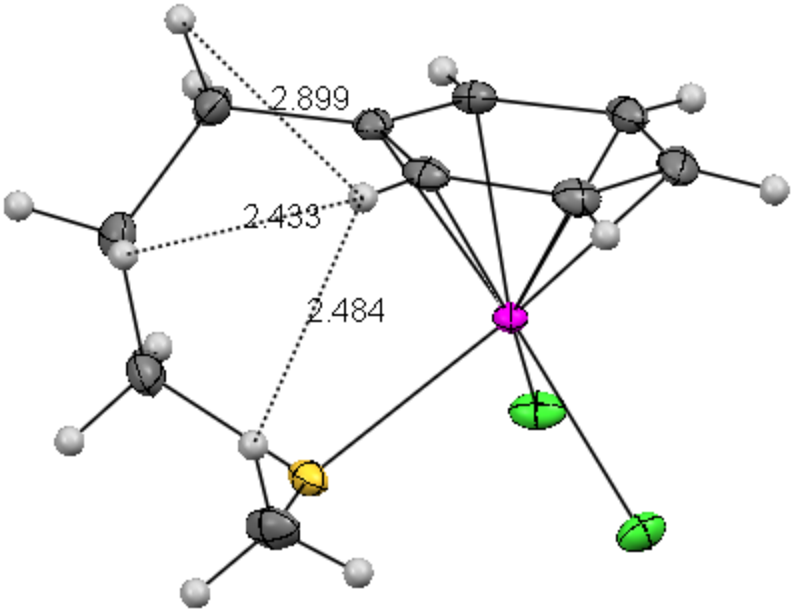

Figure S5. Crystal x-Ray structure for complex **3** with selected atom distances for NOE identification.

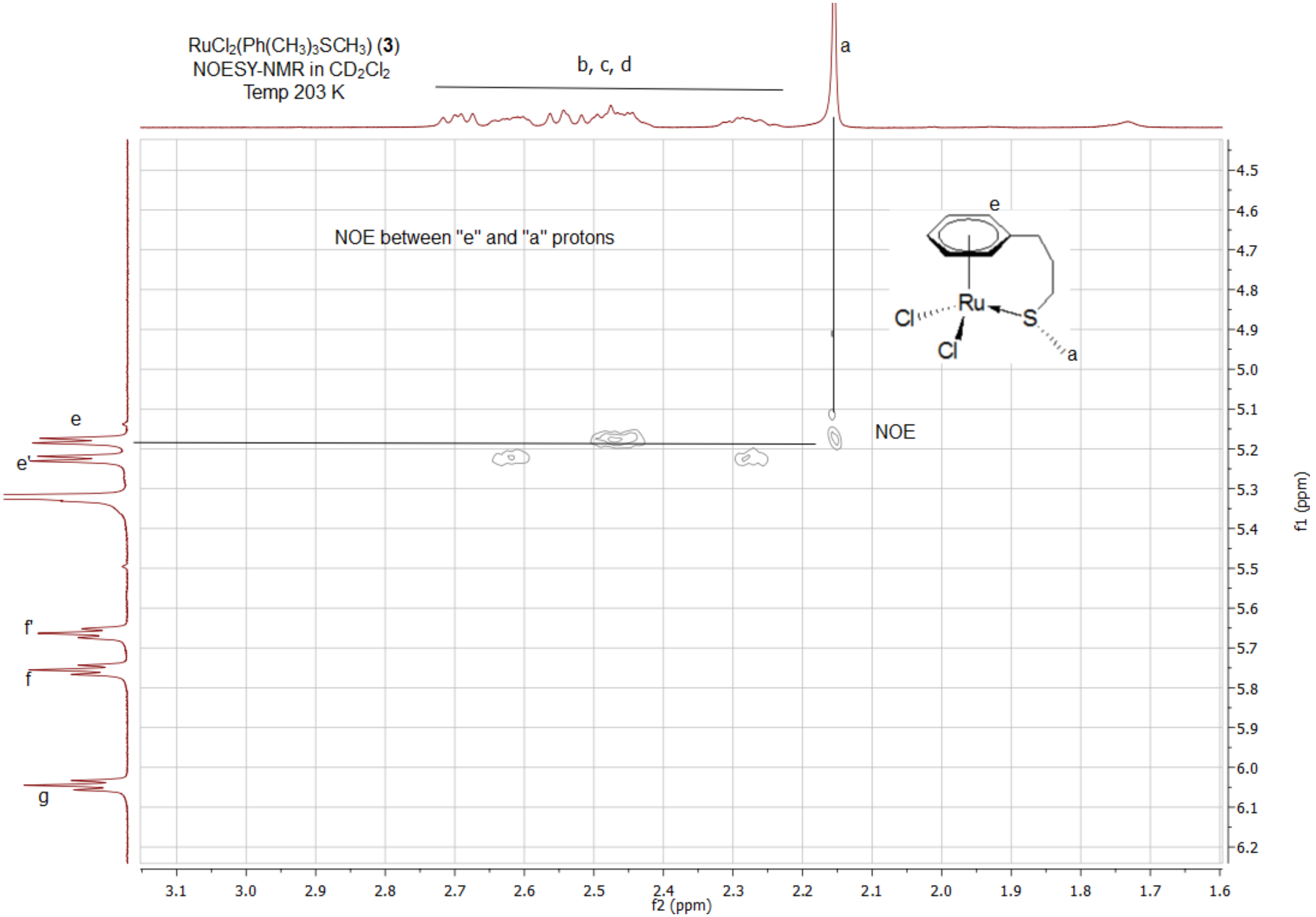

Figure S6. NOESY-NMR spectrum for complex **3** at 203 K in CD_2Cl_2

Single Crystal x-Ray Diffraction data of $RuCl_2(Ph(CH_3)_3SCH_3)$ (**3**)

X-ray Data Collection, Structure Solution and Refinement for $RuCl_2(Ph(CH_3)_3SCH_3)$ (**3**).

A red crystal of approximate dimensions 0.23 x 0.25 x 0.33 mm was mounted on a glass fiber and transferred to a Bruker SMART APEX II diffractometer. The APEX2[7] program package was used to determine the unit-cell parameters and for data collection (10 sec/frame scan time for a sphere of diffraction data). The raw frame data was processed using SAINT[8] and SADABS[9] to yield the reflection data file. Subsequent calculations were carried out using the SHELXTL[10] program. The diffraction symmetry was 2/*m* and the systematic absences were consistent with the monoclinic space group $P2_1/n$ that was later determined to be correct.

The structure was solved by direct methods and refined on F^2 by full-matrix least-squares techniques. The analytical scattering factors[11] for neutral atoms were used throughout the analysis. Hydrogen atoms were located from a difference-Fourier map and refined (x,y,z and U_{iso}).

At convergence, wR2 = 0.0413 and Goof = 1.090 for 183 variables refined against 2627 data (0.74Å), R1 = 0.0159 for those 2580 data with $I > 2.0\sigma(I)$.

Scheme S3 displays the two possible isomers for complex **3**. Figure S7 shows both isomers in the cell unit.

Scheme S3

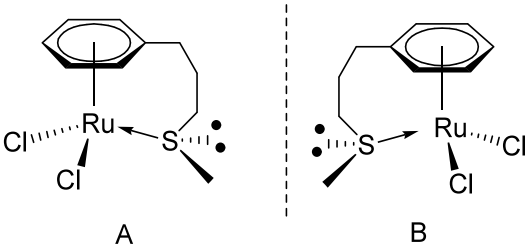

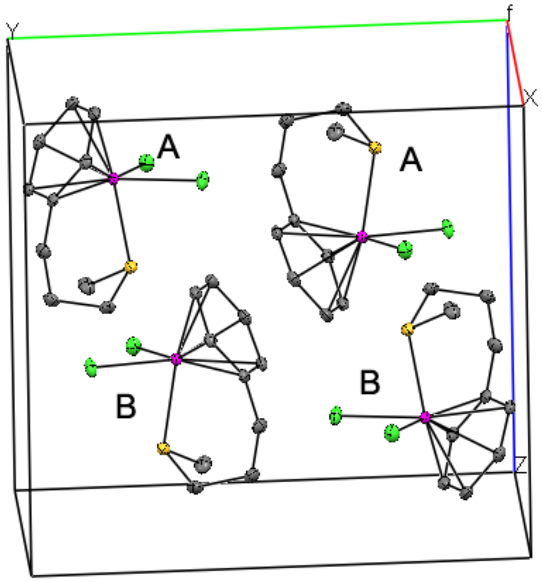

Figure S7. Unit cell for $RuCl_2(Ph(CH_3)_3SCH_3)$ **(3)** showing two different isomers A and B. Hydrogens are omitted for clarity.

Table S1. Crystal data and structure refinement for **3**.

Identification code	zg29 (Miguel Camacho)	
Empirical formula	$C_{10} H_{14} Cl_2 Ru S$	
Formula weight	338.24	
Temperature	143(2) K	
Wavelength	0.71073 Å	
Crystal system	Monoclinic	
Space group	*P*2$_1$/*n*	
Unit cell dimensions	a = 7.0069(4) Å	α= 90°.
	b = 12.8404(7) Å	β= 92.9276(5)°.
	c = 12.4298(7) Å	γ = 90°.
Volume	1116.87(11) Å^3	
Z	4	
Density (calculated)	2.012 Mg/m^3	
Absorption coefficient	2.024 mm^{-1}	
F(000)	672	
Crystal color	red	
Crystal size	0.33 x 0.25 x 0.23 mm^3	
Theta range for data collection	2.28 to 28.56°	
Index ranges	$-8 \le h \le 8$, $-16 \le k \le 17$, $-16 \le l \le 15$	

Reflections collected	12519
Independent reflections	2627 [R(int) = 0.0185]
Completeness to theta = 25.50°	100.0 %
Absorption correction	Numerical
Max. and min. transmission	0.6521 and 0.5521
Refinement method	Full-matrix least-squares on F^2
Data / restraints / parameters	2627 / 0 / 183
Goodness-of-fit on F^2	1.090
Final R indices [I>2sigma(I) = 2580 data]	R1 = 0.0159, wR2 = 0.0410
R indices (all data, 0.74Å)	R1 = 0.0163, wR2 = 0.0413
Largest diff. peak and hole	0.437 and -0.464 e.Å^{-3}

Table S2. Atomic coordinates (x 10^4) and equivalent isotropic displacement parameters (Å^{2}x 10^3) for **3**. U(eq) is defined as one third of the trace of the orthogonalized U^{ij} tensor.

	x	y	z	U(eq)
Ru(1)	1801(1)	1824(1)	8379(1)	9(1)
Cl(1)	616(1)	3575(1)	8492(1)	17(1)
Cl(2)	4904(1)	2585(1)	8110(1)	17(1)
S(1)	1327(1)	2126(1)	6506(1)	14(1)
C(1)	-594(2)	1208(1)	9225(1)	14(1)
C(2)	903(2)	1445(1)	10010(1)	15(1)
C(3)	2741(2)	1056(1)	9894(1)	16(1)
C(4)	3107(2)	397(1)	9002(1)	15(1)
C(5)	1616(2)	121(1)	8255(1)	14(1)
C(6)	-264(2)	539(1)	8354(1)	13(1)
C(7)	-1848(2)	290(1)	7531(1)	16(1)
C(8)	-1371(2)	449(1)	6357(1)	18(1)
C(9)	-971(2)	1576(1)	6065(1)	19(1)
C(10)	2926(3)	1292(1)	5816(1)	21(1)

Table S3. Bond lengths [Å] and angles [°] for **3**.

Ru(1)-Cnt	1.670
Ru(1)-C(4)	2.1729(14)
Ru(1)-C(1)	2.1738(14)
Ru(1)-C(6)	2.1941(14)
Ru(1)-C(5)	2.1952(15)
Ru(1)-C(3)	2.1975(15)
Ru(1)-C(2)	2.2073(14)
Ru(1)-S(1)	2.3670(4)
Ru(1)-Cl(1)	2.4032(4)
Ru(1)-Cl(2)	2.4228(4)
S(1)-C(10)	1.7987(17)
S(1)-C(9)	1.8165(17)
C(1)-C(6)	1.411(2)
C(1)-C(2)	1.428(2)
C(2)-C(3)	1.396(2)
C(3)-C(4)	1.428(2)
C(4)-C(5)	1.408(2)
C(5)-C(6)	1.433(2)
C(6)-C(7)	1.505(2)
C(7)-C(8)	1.527(2)
C(8)-C(9)	1.522(2)
Cnt-Ru(1)-Cl(1)	128.2
Cnt-Ru(1)-Cl(2)	129.0
Cnt-Ru(1)-S(1)	130.5
C(4)-Ru(1)-C(1)	80.94(6)
C(4)-Ru(1)-C(6)	68.67(6)
C(1)-Ru(1)-C(6)	37.69(5)
C(4)-Ru(1)-C(5)	37.59(5)
C(1)-Ru(1)-C(5)	68.14(5)
C(6)-Ru(1)-C(5)	38.12(5)
C(4)-Ru(1)-C(3)	38.15(6)
C(1)-Ru(1)-C(3)	68.11(6)
C(6)-Ru(1)-C(3)	80.97(6)

C(5)-Ru(1)-C(3)	68.12(6)
C(4)-Ru(1)-C(2)	67.74(6)
C(1)-Ru(1)-C(2)	38.03(5)
C(6)-Ru(1)-C(2)	68.18(5)
C(5)-Ru(1)-C(2)	79.99(5)
C(3)-Ru(1)-C(2)	36.94(6)
C(4)-Ru(1)-S(1)	121.62(4)
C(1)-Ru(1)-S(1)	117.54(4)
C(6)-Ru(1)-S(1)	92.87(4)
C(5)-Ru(1)-S(1)	95.12(4)
C(3)-Ru(1)-S(1)	159.66(4)
C(2)-Ru(1)-S(1)	155.12(4)
C(4)-Ru(1)-Cl(1)	155.28(4)
C(1)-Ru(1)-Cl(1)	91.98(4)
C(6)-Ru(1)-Cl(1)	118.38(4)
C(5)-Ru(1)-Cl(1)	156.44(4)
C(3)-Ru(1)-Cl(1)	117.33(4)
C(2)-Ru(1)-Cl(1)	92.14(4)
S(1)-Ru(1)-Cl(1)	82.683(13)
C(4)-Ru(1)-Cl(2)	91.42(4)
C(1)-Ru(1)-Cl(2)	159.03(4)
C(6)-Ru(1)-Cl(2)	153.82(4)
C(5)-Ru(1)-Cl(2)	116.25(4)
C(3)-Ru(1)-Cl(2)	93.87(4)
C(2)-Ru(1)-Cl(2)	121.05(4)
S(1)-Ru(1)-Cl(2)	83.103(13)
Cl(1)-Ru(1)-Cl(2)	86.879(13)
C(10)-S(1)-C(9)	100.89(8)
C(10)-S(1)-Ru(1)	108.14(6)
C(9)-S(1)-Ru(1)	108.09(5)
C(6)-C(1)-C(2)	120.70(13)
C(6)-C(1)-Ru(1)	71.94(8)
C(2)-C(1)-Ru(1)	72.26(8)
C(3)-C(2)-C(1)	120.22(14)
C(3)-C(2)-Ru(1)	71.14(9)
C(1)-C(2)-Ru(1)	69.71(8)

C(2)-C(3)-C(4)	119.65(14)
C(2)-C(3)-Ru(1)	71.91(8)
C(4)-C(3)-Ru(1)	69.99(8)
C(5)-C(4)-C(3)	120.32(14)
C(5)-C(4)-Ru(1)	72.06(8)
C(3)-C(4)-Ru(1)	71.86(8)
C(4)-C(5)-C(6)	120.24(13)
C(4)-C(5)-Ru(1)	70.34(9)
C(6)-C(5)-Ru(1)	70.90(8)
C(1)-C(6)-C(5)	118.75(13)
C(1)-C(6)-C(7)	120.46(13)
C(5)-C(6)-C(7)	120.77(13)
C(1)-C(6)-Ru(1)	70.37(8)
C(5)-C(6)-Ru(1)	70.98(8)
C(7)-C(6)-Ru(1)	129.22(10)
C(6)-C(7)-C(8)	115.54(12)
C(9)-C(8)-C(7)	114.03(13)
C(8)-C(9)-S(1)	117.99(11)

Table S4. Anisotropic displacement parameters ($Å^2$x 10^3) for **3**. The anisotropic displacement factor exponent takes the form: $-2\pi^2[h^2 a^{*2}U^{11} + ... + 2 h k a^* b^* U^{12}]$

	U^{11}	U^{22}	U^{33}	U^{23}	U^{13}	U^{12}
Ru(1)	10(1)	8(1)	10(1)	1(1)	1(1)	0(1)
Cl(1)	19(1)	10(1)	22(1)	2(1)	8(1)	3(1)
Cl(2)	12(1)	16(1)	23(1)	1(1)	2(1)	-2(1)
S(1)	20(1)	12(1)	11(1)	1(1)	1(1)	-1(1)
C(1)	15(1)	12(1)	14(1)	2(1)	4(1)	-1(1)
C(2)	23(1)	11(1)	11(1)	1(1)	2(1)	-2(1)
C(3)	21(1)	13(1)	15(1)	4(1)	-3(1)	-1(1)
C(4)	15(1)	12(1)	18(1)	5(1)	1(1)	3(1)
C(5)	18(1)	9(1)	14(1)	2(1)	4(1)	1(1)
C(6)	16(1)	10(1)	13(1)	2(1)	2(1)	-2(1)
C(7)	14(1)	16(1)	17(1)	-2(1)	0(1)	-4(1)
C(8)	19(1)	18(1)	15(1)	-3(1)	-2(1)	-3(1)
C(9)	22(1)	19(1)	14(1)	2(1)	-5(1)	0(1)
C(10)	28(1)	20(1)	17(1)	-3(1)	10(1)	-2(1)

Table S5. Hydrogen coordinates (x 10^4) and isotropic displacement parameters (Å^{2}x 10 ^{3}) for **3**.

	x	y	z	U(eq)
H(1)	-1790(30)	1526(16)	9281(16)	21(5)
H(2)	640(30)	1907(15)	10567(17)	18(5)
H(3)	3740(30)	1282(17)	10339(17)	24(5)
H(4)	4270(30)	180(16)	8892(16)	18(5)
H(5)	1920(30)	-304(16)	7667(15)	18(5)
H(7A)	-2210(30)	-444(16)	7629(15)	18(5)
H(7B)	-2940(30)	700(15)	7670(15)	18(5)
H(8A)	-370(30)	16(15)	6164(15)	16(4)
H(8B)	-2510(30)	246(16)	5935(16)	19(5)
H(9A)	-1890(30)	2024(17)	6390(17)	21(5)
H(9B)	-1000(30)	1665(16)	5308(18)	24(5)
H(10A)	2770(30)	1425(18)	5080(19)	29(5)
H(10B)	2710(30)	580(17)	5969(16)	23(5)
H(10C)	4160(30)	1470(18)	6075(18)	30(6)

Table S6. Torsion angles [°] for **3**.

C(4)-Ru(1)-S(1)-C(10)	-20.74(8)
C(1)-Ru(1)-S(1)-C(10)	-117.19(7)
C(6)-Ru(1)-S(1)-C(10)	-87.36(7)
C(5)-Ru(1)-S(1)-C(10)	-49.21(7)
C(3)-Ru(1)-S(1)-C(10)	-15.83(14)
C(2)-Ru(1)-S(1)-C(10)	-126.42(11)
Cl(1)-Ru(1)-S(1)-C(10)	154.39(6)
Cl(2)-Ru(1)-S(1)-C(10)	66.67(6)
C(4)-Ru(1)-S(1)-C(9)	87.70(8)
C(1)-Ru(1)-S(1)-C(9)	-8.76(7)
C(6)-Ru(1)-S(1)-C(9)	21.07(7)
C(5)-Ru(1)-S(1)-C(9)	59.22(7)
C(3)-Ru(1)-S(1)-C(9)	92.60(13)
C(2)-Ru(1)-S(1)-C(9)	-17.99(11)
Cl(1)-Ru(1)-S(1)-C(9)	-97.18(6)
Cl(2)-Ru(1)-S(1)-C(9)	175.10(6)
C(4)-Ru(1)-C(1)-C(6)	-66.67(9)
C(5)-Ru(1)-C(1)-C(6)	-29.86(8)
C(3)-Ru(1)-C(1)-C(6)	-104.10(9)
C(2)-Ru(1)-C(1)-C(6)	-131.92(13)
S(1)-Ru(1)-C(1)-C(6)	54.36(9)
Cl(1)-Ru(1)-C(1)-C(6)	137.14(8)
Cl(2)-Ru(1)-C(1)-C(6)	-136.41(10)
C(4)-Ru(1)-C(1)-C(2)	65.25(9)
C(6)-Ru(1)-C(1)-C(2)	131.92(13)
C(5)-Ru(1)-C(1)-C(2)	102.07(9)
C(3)-Ru(1)-C(1)-C(2)	27.83(8)
S(1)-Ru(1)-C(1)-C(2)	-173.72(7)
Cl(1)-Ru(1)-C(1)-C(2)	-90.94(8)
Cl(2)-Ru(1)-C(1)-C(2)	-4.49(16)
C(6)-C(1)-C(2)-C(3)	3.2(2)
Ru(1)-C(1)-C(2)-C(3)	-52.12(12)
C(6)-C(1)-C(2)-Ru(1)	55.35(12)
C(4)-Ru(1)-C(2)-C(3)	29.59(9)

C(1)-Ru(1)-C(2)-C(3)	133.89(13)
C(6)-Ru(1)-C(2)-C(3)	104.55(10)
C(5)-Ru(1)-C(2)-C(3)	66.73(9)
S(1)-Ru(1)-C(2)-C(3)	147.23(9)
Cl(1)-Ru(1)-C(2)-C(3)	-135.62(8)
Cl(2)-Ru(1)-C(2)-C(3)	-47.98(10)
C(4)-Ru(1)-C(2)-C(1)	-104.30(9)
C(6)-Ru(1)-C(2)-C(1)	-29.34(8)
C(5)-Ru(1)-C(2)-C(1)	-67.16(9)
C(3)-Ru(1)-C(2)-C(1)	-133.89(13)
S(1)-Ru(1)-C(2)-C(1)	13.34(15)
Cl(1)-Ru(1)-C(2)-C(1)	90.48(8)
Cl(2)-Ru(1)-C(2)-C(1)	178.13(7)
C(1)-C(2)-C(3)-C(4)	-1.7(2)
Ru(1)-C(2)-C(3)-C(4)	-53.12(12)
C(1)-C(2)-C(3)-Ru(1)	51.47(12)
C(4)-Ru(1)-C(3)-C(2)	-132.28(13)
C(1)-Ru(1)-C(3)-C(2)	-28.58(9)
C(6)-Ru(1)-C(3)-C(2)	-65.48(9)
C(5)-Ru(1)-C(3)-C(2)	-102.86(10)
S(1)-Ru(1)-C(3)-C(2)	-139.06(11)
Cl(1)-Ru(1)-C(3)-C(2)	51.88(9)
Cl(2)-Ru(1)-C(3)-C(2)	140.36(8)
C(1)-Ru(1)-C(3)-C(4)	103.70(10)
C(6)-Ru(1)-C(3)-C(4)	66.80(9)
C(5)-Ru(1)-C(3)-C(4)	29.43(9)
C(2)-Ru(1)-C(3)-C(4)	132.28(13)
S(1)-Ru(1)-C(3)-C(4)	-6.77(18)
Cl(1)-Ru(1)-C(3)-C(4)	-175.84(7)
Cl(2)-Ru(1)-C(3)-C(4)	-87.35(9)
C(2)-C(3)-C(4)-C(5)	-1.4(2)
Ru(1)-C(3)-C(4)-C(5)	-55.45(12)
C(2)-C(3)-C(4)-Ru(1)	54.02(12)
C(1)-Ru(1)-C(4)-C(5)	65.74(9)
C(6)-Ru(1)-C(4)-C(5)	28.68(8)
C(3)-Ru(1)-C(4)-C(5)	131.64(13)

C(2)-Ru(1)-C(4)-C(5)	102.93(9)
S(1)-Ru(1)-C(4)-C(5)	-51.11(9)
Cl(1)-Ru(1)-C(4)-C(5)	140.51(9)
Cl(2)-Ru(1)-C(4)-C(5)	-133.88(8)
C(1)-Ru(1)-C(4)-C(3)	-65.91(9)
C(6)-Ru(1)-C(4)-C(3)	-102.97(10)
C(5)-Ru(1)-C(4)-C(3)	-131.65(13)
C(2)-Ru(1)-C(4)-C(3)	-28.72(9)
S(1)-Ru(1)-C(4)-C(3)	177.24(7)
Cl(1)-Ru(1)-C(4)-C(3)	8.86(16)
Cl(2)-Ru(1)-C(4)-C(3)	94.47(9)
C(3)-C(4)-C(5)-C(6)	3.0(2)
Ru(1)-C(4)-C(5)-C(6)	-52.38(12)
C(3)-C(4)-C(5)-Ru(1)	55.35(12)
C(1)-Ru(1)-C(5)-C(4)	-104.06(9)
C(6)-Ru(1)-C(5)-C(4)	-133.60(12)
C(3)-Ru(1)-C(5)-C(4)	-29.83(9)
C(2)-Ru(1)-C(5)-C(4)	-66.34(9)
S(1)-Ru(1)-C(5)-C(4)	138.28(8)
Cl(1)-Ru(1)-C(5)-C(4)	-138.29(9)
Cl(2)-Ru(1)-C(5)-C(4)	53.46(9)
C(4)-Ru(1)-C(5)-C(6)	133.60(12)
C(1)-Ru(1)-C(5)-C(6)	29.54(8)
C(3)-Ru(1)-C(5)-C(6)	103.77(9)
C(2)-Ru(1)-C(5)-C(6)	67.26(9)
S(1)-Ru(1)-C(5)-C(6)	-88.12(8)
Cl(1)-Ru(1)-C(5)-C(6)	-4.69(15)
Cl(2)-Ru(1)-C(5)-C(6)	-172.94(7)
C(2)-C(1)-C(6)-C(5)	-1.7(2)
Ru(1)-C(1)-C(6)-C(5)	53.82(11)
C(2)-C(1)-C(6)-C(7)	179.81(13)
Ru(1)-C(1)-C(6)-C(7)	-124.68(13)
C(2)-C(1)-C(6)-Ru(1)	-55.50(12)
C(4)-C(5)-C(6)-C(1)	-1.4(2)
Ru(1)-C(5)-C(6)-C(1)	-53.53(11)
C(4)-C(5)-C(6)-C(7)	177.10(13)

Ru(1)-C(5)-C(6)-C(7)	124.97(13)
C(4)-C(5)-C(6)-Ru(1)	52.13(12)
C(4)-Ru(1)-C(6)-C(1)	103.23(9)
C(5)-Ru(1)-C(6)-C(1)	131.54(12)
C(3)-Ru(1)-C(6)-C(1)	65.68(9)
C(2)-Ru(1)-C(6)-C(1)	29.59(8)
S(1)-Ru(1)-C(6)-C(1)	-133.82(8)
Cl(1)-Ru(1)-C(6)-C(1)	-50.59(9)
Cl(2)-Ru(1)-C(6)-C(1)	146.00(8)
C(4)-Ru(1)-C(6)-C(5)	-28.31(8)
C(1)-Ru(1)-C(6)-C(5)	-131.54(12)
C(3)-Ru(1)-C(6)-C(5)	-65.86(9)
C(2)-Ru(1)-C(6)-C(5)	-101.95(9)
S(1)-Ru(1)-C(6)-C(5)	94.64(8)
Cl(1)-Ru(1)-C(6)-C(5)	177.87(7)
Cl(2)-Ru(1)-C(6)-C(5)	14.47(14)
C(4)-Ru(1)-C(6)-C(7)	-142.96(14)
C(1)-Ru(1)-C(6)-C(7)	113.81(16)
C(5)-Ru(1)-C(6)-C(7)	-114.65(16)
C(3)-Ru(1)-C(6)-C(7)	179.49(14)
C(2)-Ru(1)-C(6)-C(7)	143.40(14)
S(1)-Ru(1)-C(6)-C(7)	-20.01(13)
Cl(1)-Ru(1)-C(6)-C(7)	63.22(14)
Cl(2)-Ru(1)-C(6)-C(7)	-100.19(14)
C(1)-C(6)-C(7)-C(8)	128.62(15)
C(5)-C(6)-C(7)-C(8)	-49.85(19)
Ru(1)-C(6)-C(7)-C(8)	39.94(19)
C(6)-C(7)-C(8)-C(9)	-64.58(18)
C(7)-C(8)-C(9)-S(1)	76.13(17)
C(10)-S(1)-C(9)-C(8)	61.47(14)
Ru(1)-S(1)-C(9)-C(8)	-51.88(13)

Complex $Ru(CH_3)_2(Ph(CH_3)_3SCH_3)$ (4): Synthesis and Characterization

Scheme S4

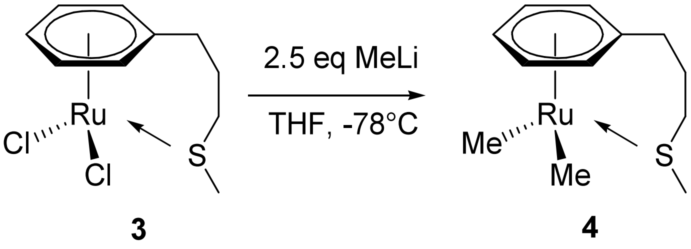

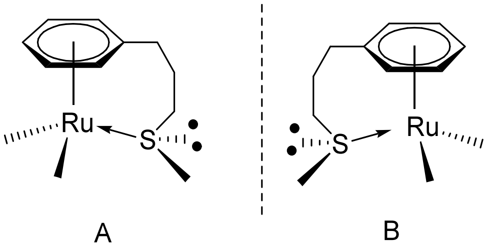

Synthesis of [Ru(η^6- $Ph(CH_2)_3S(CH_3)_2(CH_3)_2$] (4). 0.2000 g (0.591 mmol, 1 eq) of **3** were suspended on 20ml of THF (in glove box) sonicated and stirred for 10 minutes. Outside glove box the solution was cooled down to -78°C. MeLi was added from a 1.6M solution in ether 0.94 ml (1.5 mmol, 2.5 eq). MeLi solution was added through needle dropwise. Solution was allowed to reach 10°C but not higher. Solution turns dark red when it reaches 10°C and then it is dried under high vacuum to eliminate THF keeping temperature under 10°C. Flask was introduced in the glove box and red dark solid was dissolved in ether. Ether solution was filtrated through celite and Florisyl (plug). Drying of solution afforded yellow crystalline material. Golden crystals suitable for analysis were obtained from a DCM solution by slow evaporation. Complex **4** is very unstable and must be kept under inert atmosphere. Yield: 0.0352 g, 20%. ^{1}H

NMR (500 MHz, CD_2Cl_2, 183K): δ 5.10 (b, 1H,), 4.99 (b, 1H), 4.95 (b, 1H), 4.85 (b, 1H), 4.23 (b, 1H). 2.80 (d, 7.0 Hz, 1H), 2.56 (m, 1H), 1.97 (s, 3H), 1.95-1.58 (m, 6H), -0.17 (s, 3H), -0.27 (s, 3H). ^{13}C NMR (500 MHz, $CDCl_3$, 183K): δ 95.3, 92.0, 91.4, 84.1, 82.4, 72.6, 33.8, 30.9, 23.3, 21.9, -7.32, -9.89.HRMS (ESI+, CH_2Cl_2) *m/z* calcd for $C_{12}H_{20}SRu$ $[M]^+$, 297.42; found $[M-CH_3]^+$, 283.01.

1D and 2D NMR Characterization of Complex 4

Figures S8 to S13 depict a series of 1D and 2D NMR experiments (^{1}H-NMR, ^{13}C-NMR, HMQC, COSY, NOE) at 183 K to fully assign all peaks. Ethylene was flushed through the solution to see the effect on complex **4** before activation. No coordination of ethylene or sulfur displacement is observed.

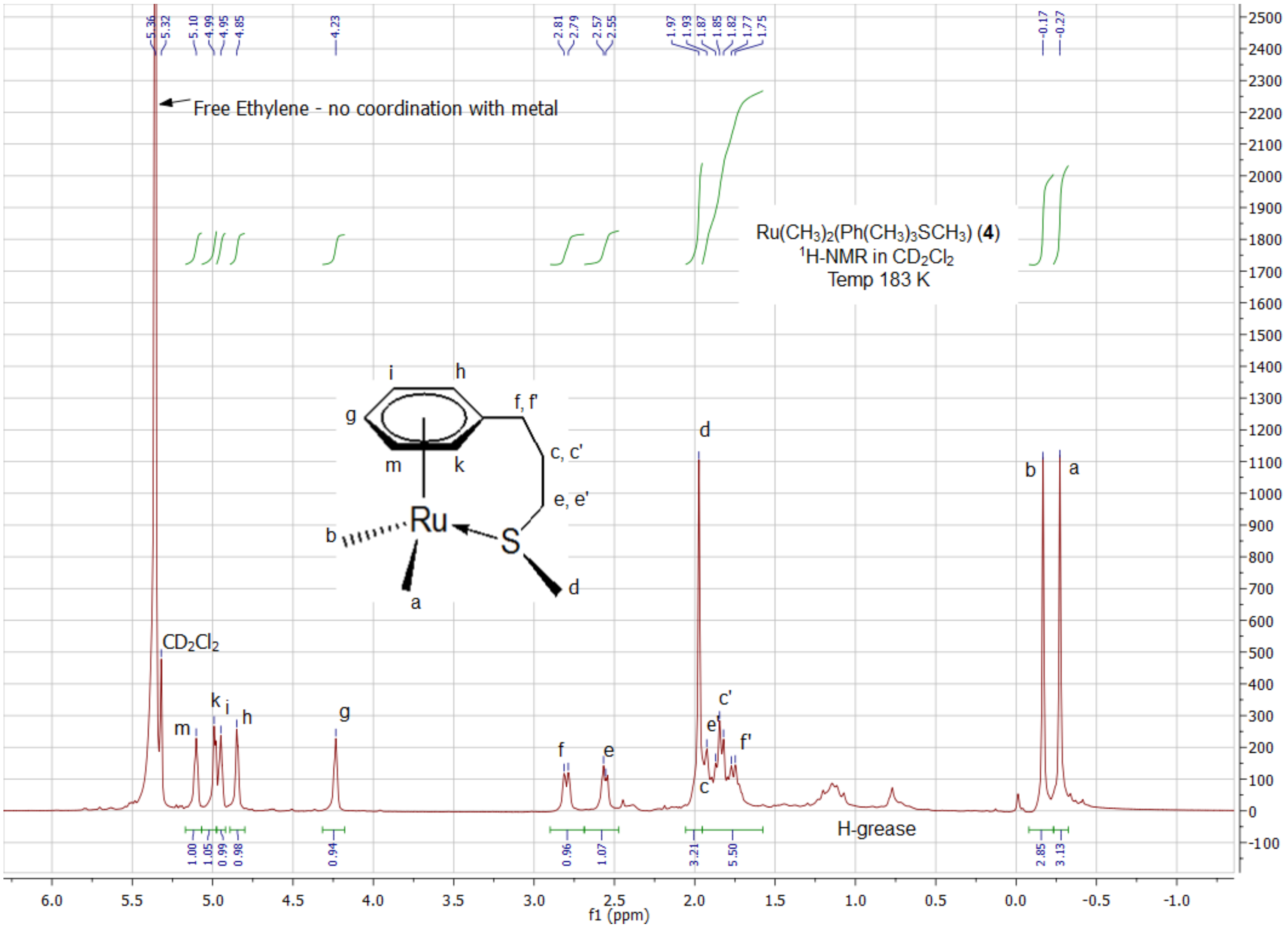

Figure S8. ^{1}H-NMR spectrum of complex **4** at 183 K in CD_2Cl_2.

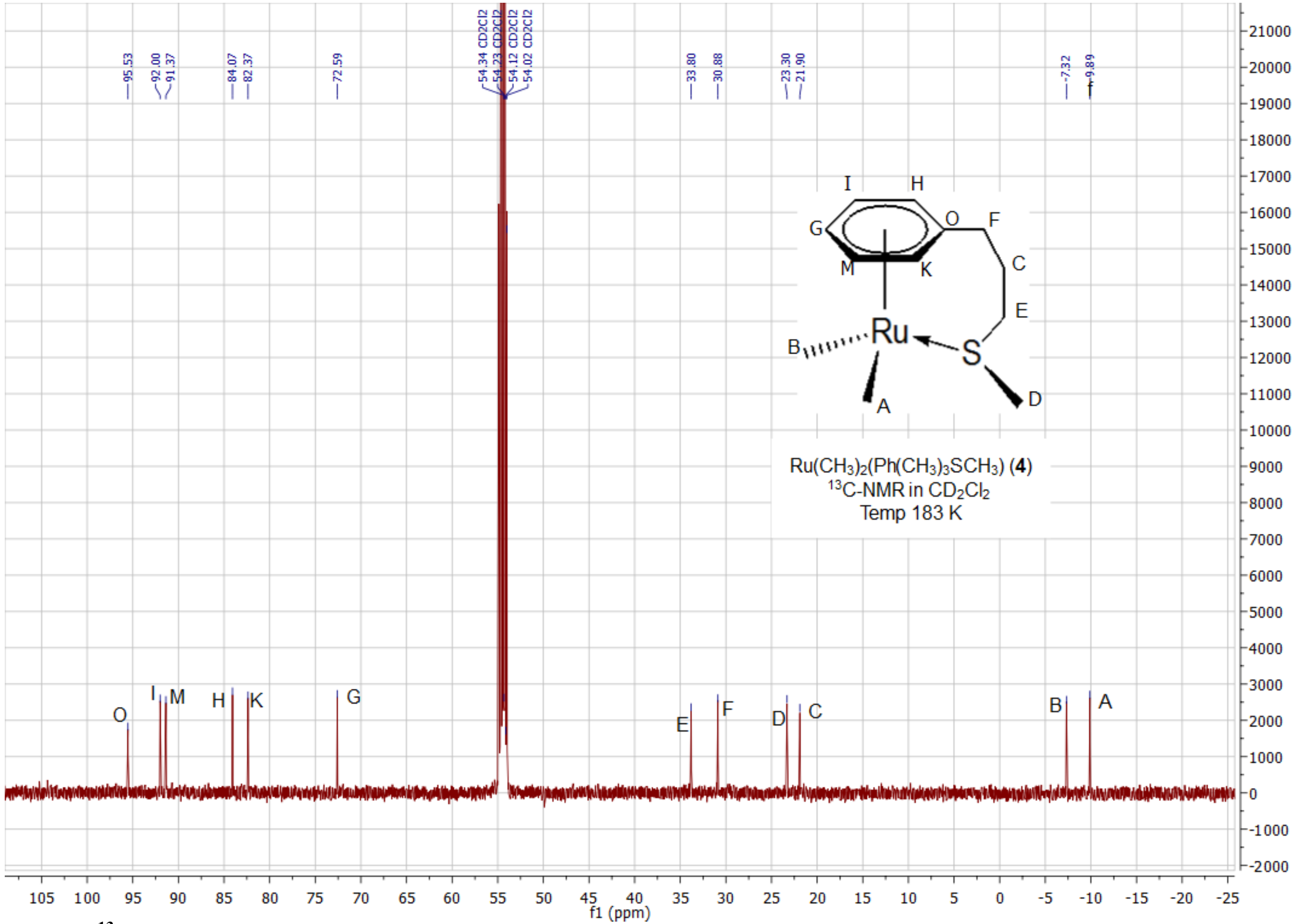

Figure S9. ^{13}C-NMR spectrum of complex **4** at 183 K in CD_2Cl_2.

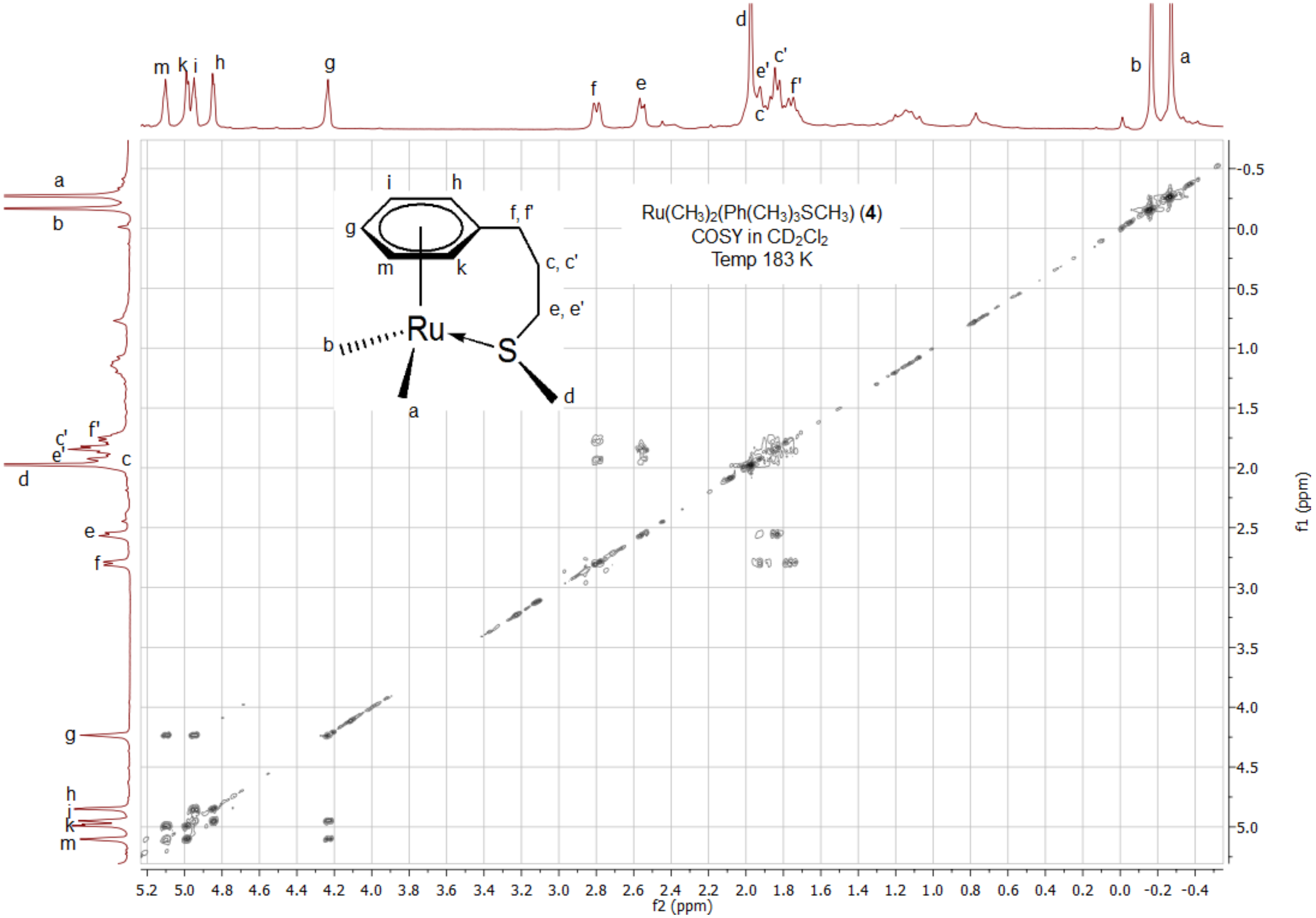

Figure S10. COSY-NMR spectrum of complex **4** at 183 K in CD_2Cl_2.

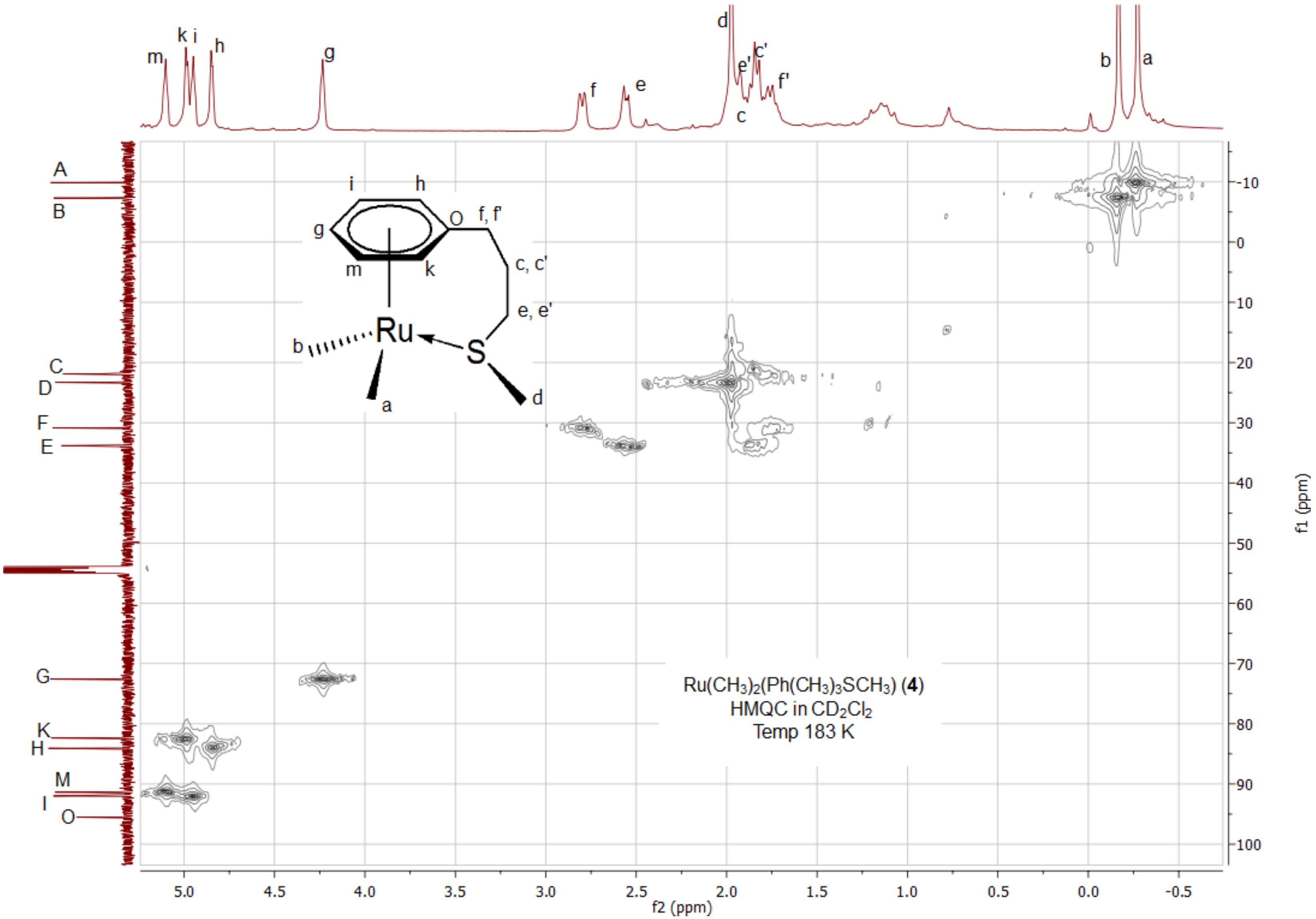

Figure S11. HMQC-NMR spectrum of complex **4** at 183 K in CD_2Cl_2.

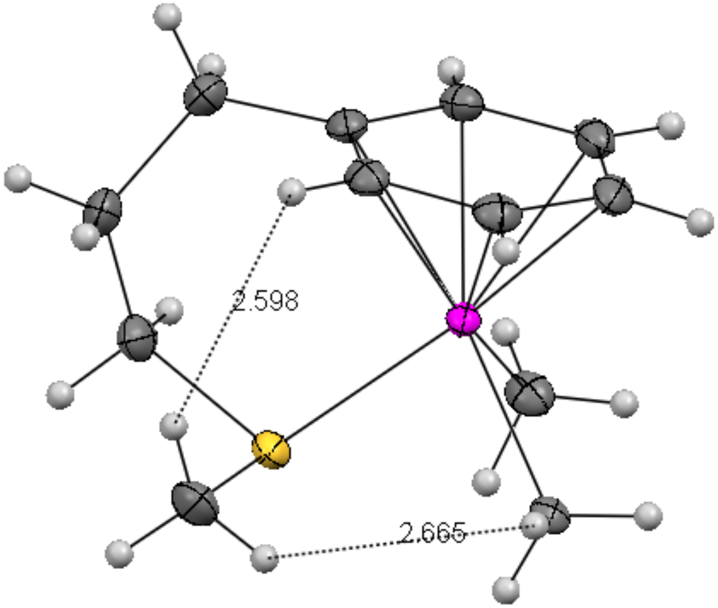

Figure S12. X-Ray crystal structure of complex **4** with selected atom distances for NOE identification.

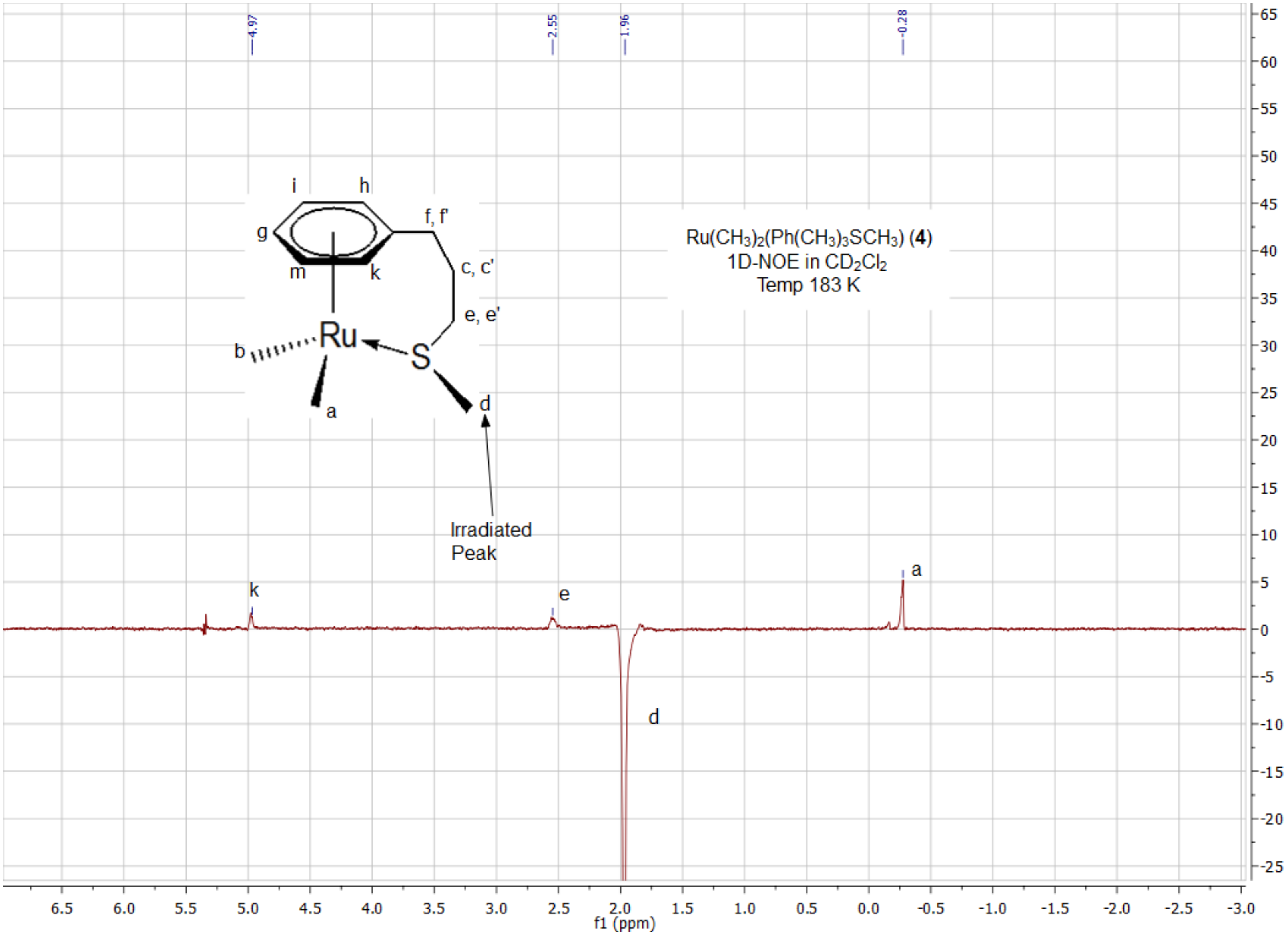

Figure S13. NOE-NMR spectrum of complex **4** at 183 K in CD_2Cl_2.

Single Crystal x-Ray Diffraction Data of Complex **4**

X-ray Data Collection, Structure Solution and Refinement for $Ru(CH_3)_2(Ph(CH_3)_3SCH_3)$ (**4**).

A gold crystal of approximate dimensions 0.17 x 0.20 x 0.22 mm was mounted on a glass fiber and transferred to a Bruker SMART APEX II diffractometer. The APEX2[7] program package was used to determine the unit-cell parameters and for data collection (20 sec/frame scan time for a sphere of diffraction data). The raw frame data was processed using SAINT[8] and SADABS[9] to yield the reflection data file. Subsequent calculations were carried out using the SHELXTL[10] program. The diffraction symmetry was 2/*m* and the systematic absences were consistent with the monoclinic space group $P2_1/n$ that was later determined to be correct.

The structure was solved by direct methods and refined on F^2 by full-matrix least-squares techniques. The analytical scattering factors[11] for neutral atoms were used throughout the analysis. Hydrogen atoms were either located from a difference-Fourier map and refined (x,y,z and U_{iso}) or were included using a riding model.

At convergence, wR2 = 0.0422 and Goof = 1.092 for 196 variables refined against 2930 data (0.74Å), R1 = 0.0171 for those 2831 data with $I > 2.0\sigma(I)$.

Table S7. Crystal data and structure refinement for $Ru(CH_3)_2(Ph(CH_3)_3SCH_3)$ (**4**).

Empirical formula	$C_{12} H_{20}$ Ru S	
Formula weight	297.41	
Temperature	88(2) K	
Wavelength	0.71073 Å	
Crystal system	Monoclinic	
Space group	$P2_{(1)}/n$	
Unit cell dimensions	a = 6.8375(3) Å	α= 90°.
	b = 13.5463(5) Å	β= 93.8780(4)°.
	c = 12.8712(5) Å	γ = 90°.
Volume	1189.44(8) $Å^3$	
Z	4	
Density (calculated)	1.661 Mg/m^3	
Absorption coefficient	1.454 mm^{-1}	
F(000)	608	
Crystal color	gold	
Crystal size	0.22 x 0.20 x 0.17 mm^3	
Theta range for data collection	2.19 to 28.77°	
Index ranges	$-9 \le h \le 9$, $-18 \le k \le 17$, $-16 \le l \le 17$	

Reflections collected	13876
Independent reflections	2930 [R(int) = 0.0130]
Completeness to theta = 25.50°	100.0 %
Absorption correction	Numerical
Max. and min. transmission	0.7944 and 0.7452
Refinement method	Full-matrix least-squares on F^2
Data / restraints / parameters	2930 / 0 / 196
Goodness-of-fit on F^2	1.092
Final R indices [I>2sigma(I) = 2831 data]	R1 = 0.0171, wR2 = 0.0418
R indices (all data, 0.74Å)	R1 = 0.0179, wR2 = 0.0422
Largest diff. peak and hole	0.731 and -0.339 e.Å^{-3}

Table S8. Atomic coordinates (x 10^4) and equivalent isotropic displacement parameters (Å^{2}x 10^3) for $Ru(CH_3)_2(Ph(CH_3)_3SCH_3)$ (**4**). U(eq) is defined as one third of the trace of the orthogonalized U^{ij} tensor.

	x	y	z	U(eq)
Ru(1)	1673(1)	1825(1)	3405(1)	12(1)
S(1)	1114(1)	2045(1)	1623(1)	17(1)
C(1)	-721(3)	1172(1)	4264(1)	18(1)
C(2)	817(3)	1502(1)	4988(1)	19(1)
C(3)	2750(3)	1179(1)	4904(1)	20(1)
C(4)	3166(3)	491(1)	4105(1)	19(1)
C(5)	1660(3)	161(1)	3401(1)	18(1)
C(6)	-300(2)	521(1)	3451(1)	16(1)
C(7)	-1895(3)	209(1)	2649(1)	21(1)
C(8)	-1459(3)	375(1)	1508(1)	22(1)
C(9)	-1189(3)	1450(1)	1198(1)	22(1)
C(10)	2796(3)	1286(2)	950(2)	25(1)
C(11)	550(3)	3296(1)	3481(1)	21(1)
C(12)	4421(2)	2624(1)	3182(1)	14(1)

Table S9. Bond lengths [Å] and angles [°] for Ru(CH_3)$_2$(Ph(CH_3)$_3$SCH_3) (**4**).

Ru(1)-Cnt	1.712
Ru(1)-C(11)	2.1411(17)
Ru(1)-C(3)	2.2004(16)
Ru(1)-C(2)	2.2016(17)
Ru(1)-C(12)	2.2041(16)
Ru(1)-C(1)	2.2197(16)
Ru(1)-C(6)	2.2253(16)
Ru(1)-C(4)	2.2351(16)
Ru(1)-C(5)	2.2532(17)
Ru(1)-S(1)	2.3187(4)
S(1)-C(10)	1.807(2)
S(1)-C(9)	1.8197(18)
C(1)-C(6)	1.412(2)
C(1)-C(2)	1.428(2)
C(2)-C(3)	1.403(3)
C(3)-C(4)	1.431(2)
C(4)-C(5)	1.398(2)
C(5)-C(6)	1.432(2)
C(6)-C(7)	1.510(2)
C(7)-C(8)	1.534(2)
C(8)-C(9)	1.525(3)
Cnt-Ru(1)-S(1)	131.1
Cnt-Ru(1)-C(11)	128.4
Cnt-Ru(1)-C(12)	130.3
C(11)-Ru(1)-C(3)	115.44(7)
C(11)-Ru(1)-C(2)	91.35(7)
C(3)-Ru(1)-C(2)	37.18(7)
C(11)-Ru(1)-C(12)	81.97(7)
C(3)-Ru(1)-C(12)	94.10(6)
C(2)-Ru(1)-C(12)	120.02(6)
C(11)-Ru(1)-C(1)	93.96(7)
C(3)-Ru(1)-C(1)	67.60(6)
C(2)-Ru(1)-C(1)	37.69(6)

C(12)-Ru(1)-C(1)	157.54(6)
C(11)-Ru(1)-C(6)	121.17(7)
C(3)-Ru(1)-C(6)	80.13(6)
C(2)-Ru(1)-C(6)	67.54(6)
C(12)-Ru(1)-C(6)	156.47(6)
C(1)-Ru(1)-C(6)	37.05(6)
C(11)-Ru(1)-C(4)	152.81(7)
C(3)-Ru(1)-C(4)	37.63(6)
C(2)-Ru(1)-C(4)	66.97(6)
C(12)-Ru(1)-C(4)	94.54(6)
C(1)-Ru(1)-C(4)	79.00(6)
C(6)-Ru(1)-C(4)	66.98(6)
C(11)-Ru(1)-C(5)	158.42(7)
C(3)-Ru(1)-C(5)	66.75(6)
C(2)-Ru(1)-C(5)	78.59(6)
C(12)-Ru(1)-C(5)	119.60(6)
C(1)-Ru(1)-C(5)	66.42(6)
C(6)-Ru(1)-C(5)	37.29(6)
C(4)-Ru(1)-C(5)	36.30(6)
C(11)-Ru(1)-S(1)	83.70(5)
C(3)-Ru(1)-S(1)	160.36(5)
C(2)-Ru(1)-S(1)	154.79(5)
C(12)-Ru(1)-S(1)	83.86(4)
C(1)-Ru(1)-S(1)	117.80(5)
C(6)-Ru(1)-S(1)	93.96(4)
C(4)-Ru(1)-S(1)	122.91(5)
C(5)-Ru(1)-S(1)	97.26(4)
C(10)-S(1)-C(9)	99.81(9)
C(10)-S(1)-Ru(1)	109.44(7)
C(9)-S(1)-Ru(1)	108.76(6)
C(6)-C(1)-C(2)	120.05(16)
C(6)-C(1)-Ru(1)	71.69(9)
C(2)-C(1)-Ru(1)	70.47(9)
C(3)-C(2)-C(1)	120.53(16)
C(3)-C(2)-Ru(1)	71.36(10)
C(1)-C(2)-Ru(1)	71.84(9)

C(2)-C(3)-C(4)	119.49(16)
C(2)-C(3)-Ru(1)	71.45(10)
C(4)-C(3)-Ru(1)	72.50(9)
C(5)-C(4)-C(3)	120.03(16)
C(5)-C(4)-Ru(1)	72.55(10)
C(3)-C(4)-Ru(1)	69.87(9)
C(4)-C(5)-C(6)	120.85(16)
C(4)-C(5)-Ru(1)	71.15(10)
C(6)-C(5)-Ru(1)	70.30(9)
C(1)-C(6)-C(5)	118.94(15)
C(1)-C(6)-C(7)	120.49(15)
C(5)-C(6)-C(7)	120.58(15)
C(1)-C(6)-Ru(1)	71.26(9)
C(5)-C(6)-Ru(1)	72.41(9)
C(7)-C(6)-Ru(1)	127.93(11)
C(6)-C(7)-C(8)	115.79(14)
C(9)-C(8)-C(7)	115.19(15)
C(8)-C(9)-S(1)	117.48(13)

Table S10. Torsion angles [°] for Ru(CH$_3$)$_2$(Ph(CH$_3$)$_3$SCH$_3$) (**4**).

C(11)-Ru(1)-S(1)-C(10)	152.40(9)
C(3)-Ru(1)-S(1)-C(10)	-15.14(16)
C(2)-Ru(1)-S(1)-C(10)	-127.90(13)
C(12)-Ru(1)-S(1)-C(10)	69.84(8)
C(1)-Ru(1)-S(1)-C(10)	-116.43(9)
C(6)-Ru(1)-S(1)-C(10)	-86.64(8)
C(4)-Ru(1)-S(1)-C(10)	-21.60(9)
C(5)-Ru(1)-S(1)-C(10)	-49.31(8)
C(11)-Ru(1)-S(1)-C(9)	-99.50(9)
C(3)-Ru(1)-S(1)-C(9)	92.96(16)
C(2)-Ru(1)-S(1)-C(9)	-19.80(13)
C(12)-Ru(1)-S(1)-C(9)	177.93(8)
C(1)-Ru(1)-S(1)-C(9)	-8.34(9)
C(6)-Ru(1)-S(1)-C(9)	21.46(8)

C(4)-Ru(1)-S(1)-C(9)	86.49(9)
C(5)-Ru(1)-S(1)-C(9)	58.79(8)
C(11)-Ru(1)-C(1)-C(6)	140.30(10)
C(3)-Ru(1)-C(1)-C(6)	-103.78(11)
C(2)-Ru(1)-C(1)-C(6)	-132.62(15)
C(12)-Ru(1)-C(1)-C(6)	-141.17(14)
C(4)-Ru(1)-C(1)-C(6)	-66.20(10)
C(5)-Ru(1)-C(1)-C(6)	-30.39(9)
S(1)-Ru(1)-C(1)-C(6)	55.34(10)
C(11)-Ru(1)-C(1)-C(2)	-87.08(11)
C(3)-Ru(1)-C(1)-C(2)	28.84(10)
C(12)-Ru(1)-C(1)-C(2)	-8.6(2)
C(6)-Ru(1)-C(1)-C(2)	132.62(15)
C(4)-Ru(1)-C(1)-C(2)	66.42(10)
C(5)-Ru(1)-C(1)-C(2)	102.22(11)
S(1)-Ru(1)-C(1)-C(2)	-172.04(8)
C(6)-C(1)-C(2)-C(3)	-0.5(2)
Ru(1)-C(1)-C(2)-C(3)	-54.28(14)
C(6)-C(1)-C(2)-Ru(1)	53.81(14)
C(11)-Ru(1)-C(2)-C(3)	-132.83(11)
C(12)-Ru(1)-C(2)-C(3)	-51.32(12)
C(1)-Ru(1)-C(2)-C(3)	132.44(15)
C(6)-Ru(1)-C(2)-C(3)	103.77(11)
C(4)-Ru(1)-C(2)-C(3)	30.27(10)
C(5)-Ru(1)-C(2)-C(3)	66.40(11)
S(1)-Ru(1)-C(2)-C(3)	149.15(10)
C(11)-Ru(1)-C(2)-C(1)	94.73(11)
C(3)-Ru(1)-C(2)-C(1)	-132.44(15)
C(12)-Ru(1)-C(2)-C(1)	176.24(9)
C(6)-Ru(1)-C(2)-C(1)	-28.67(10)
C(4)-Ru(1)-C(2)-C(1)	-102.17(11)
C(5)-Ru(1)-C(2)-C(1)	-66.03(10)
S(1)-Ru(1)-C(2)-C(1)	16.71(17)
C(1)-C(2)-C(3)-C(4)	-1.9(2)
Ru(1)-C(2)-C(3)-C(4)	-56.36(14)
C(1)-C(2)-C(3)-Ru(1)	54.50(14)

C(11)-Ru(1)-C(3)-C(2)	54.28(12)
C(12)-Ru(1)-C(3)-C(2)	137.34(10)
C(1)-Ru(1)-C(3)-C(2)	-29.21(10)
C(6)-Ru(1)-C(3)-C(2)	-65.66(10)
C(4)-Ru(1)-C(3)-C(2)	-130.55(15)
C(5)-Ru(1)-C(3)-C(2)	-102.13(11)
S(1)-Ru(1)-C(3)-C(2)	-139.46(13)
C(11)-Ru(1)-C(3)-C(4)	-175.17(10)
C(2)-Ru(1)-C(3)-C(4)	130.55(15)
C(12)-Ru(1)-C(3)-C(4)	-92.11(10)
C(1)-Ru(1)-C(3)-C(4)	101.34(11)
C(6)-Ru(1)-C(3)-C(4)	64.89(10)
C(5)-Ru(1)-C(3)-C(4)	28.42(10)
S(1)-Ru(1)-C(3)-C(4)	-8.9(2)
C(2)-C(3)-C(4)-C(5)	1.4(2)
Ru(1)-C(3)-C(4)-C(5)	-54.50(14)
C(2)-C(3)-C(4)-Ru(1)	55.85(14)
C(11)-Ru(1)-C(4)-C(5)	141.95(15)
C(3)-Ru(1)-C(4)-C(5)	132.37(15)
C(2)-Ru(1)-C(4)-C(5)	102.44(11)
C(12)-Ru(1)-C(4)-C(5)	-136.79(10)
C(1)-Ru(1)-C(4)-C(5)	64.93(10)
C(6)-Ru(1)-C(4)-C(5)	28.13(10)
S(1)-Ru(1)-C(4)-C(5)	-51.18(11)
C(11)-Ru(1)-C(4)-C(3)	9.6(2)
C(2)-Ru(1)-C(4)-C(3)	-29.93(10)
C(12)-Ru(1)-C(4)-C(3)	90.84(11)
C(1)-Ru(1)-C(4)-C(3)	-67.44(11)
C(6)-Ru(1)-C(4)-C(3)	-104.24(11)
C(5)-Ru(1)-C(4)-C(3)	-132.37(15)
S(1)-Ru(1)-C(4)-C(3)	176.45(8)
C(3)-C(4)-C(5)-C(6)	1.5(2)
Ru(1)-C(4)-C(5)-C(6)	-51.77(14)
C(3)-C(4)-C(5)-Ru(1)	53.25(14)
C(11)-Ru(1)-C(5)-C(4)	-130.04(18)
C(3)-Ru(1)-C(5)-C(4)	-29.40(10)

C(2)-Ru(1)-C(5)-C(4)	-66.47(11)
C(12)-Ru(1)-C(5)-C(4)	51.71(12)
C(1)-Ru(1)-C(5)-C(4)	-104.03(11)
C(6)-Ru(1)-C(5)-C(4)	-134.25(15)
S(1)-Ru(1)-C(5)-C(4)	138.75(9)
C(11)-Ru(1)-C(5)-C(6)	4.2(2)
C(3)-Ru(1)-C(5)-C(6)	104.85(11)
C(2)-Ru(1)-C(5)-C(6)	67.78(10)
C(12)-Ru(1)-C(5)-C(6)	-174.04(9)
C(1)-Ru(1)-C(5)-C(6)	30.21(9)
C(4)-Ru(1)-C(5)-C(6)	134.25(15)
S(1)-Ru(1)-C(5)-C(6)	-87.01(9)
C(2)-C(1)-C(6)-C(5)	3.2(2)
Ru(1)-C(1)-C(6)-C(5)	56.49(13)
C(2)-C(1)-C(6)-C(7)	-176.85(15)
Ru(1)-C(1)-C(6)-C(7)	-123.60(15)
C(2)-C(1)-C(6)-Ru(1)	-53.25(14)
C(4)-C(5)-C(6)-C(1)	-3.8(2)
Ru(1)-C(5)-C(6)-C(1)	-55.92(13)
C(4)-C(5)-C(6)-C(7)	176.32(15)
Ru(1)-C(5)-C(6)-C(7)	124.17(15)
C(4)-C(5)-C(6)-Ru(1)	52.15(14)
C(11)-Ru(1)-C(6)-C(1)	-48.14(12)
C(3)-Ru(1)-C(6)-C(1)	65.71(10)
C(2)-Ru(1)-C(6)-C(1)	29.14(10)
C(12)-Ru(1)-C(6)-C(1)	143.13(14)
C(4)-Ru(1)-C(6)-C(1)	102.62(11)
C(5)-Ru(1)-C(6)-C(1)	130.06(14)
S(1)-Ru(1)-C(6)-C(1)	-133.17(9)
C(11)-Ru(1)-C(6)-C(5)	-178.19(9)
C(3)-Ru(1)-C(6)-C(5)	-64.35(10)
C(2)-Ru(1)-C(6)-C(5)	-100.92(11)
C(12)-Ru(1)-C(6)-C(5)	13.07(19)
C(1)-Ru(1)-C(6)-C(5)	-130.06(14)
C(4)-Ru(1)-C(6)-C(5)	-27.43(9)
S(1)-Ru(1)-C(6)-C(5)	96.78(9)

C(11)-Ru(1)-C(6)-C(7)	66.37(17)
C(3)-Ru(1)-C(6)-C(7)	-179.79(16)
C(2)-Ru(1)-C(6)-C(7)	143.64(17)
C(12)-Ru(1)-C(6)-C(7)	-102.37(19)
C(1)-Ru(1)-C(6)-C(7)	114.51(19)
C(4)-Ru(1)-C(6)-C(7)	-142.87(17)
C(5)-Ru(1)-C(6)-C(7)	-115.44(19)
S(1)-Ru(1)-C(6)-C(7)	-18.66(15)
C(1)-C(6)-C(7)-C(8)	126.25(18)
C(5)-C(6)-C(7)-C(8)	-53.8(2)
Ru(1)-C(6)-C(7)-C(8)	37.1(2)
C(6)-C(7)-C(8)-C(9)	-63.2(2)
C(7)-C(8)-C(9)-S(1)	75.66(19)
C(10)-S(1)-C(9)-C(8)	62.43(16)
Ru(1)-S(1)-C(9)-C(8)	-52.12(15)

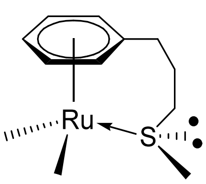

A

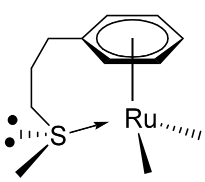

B

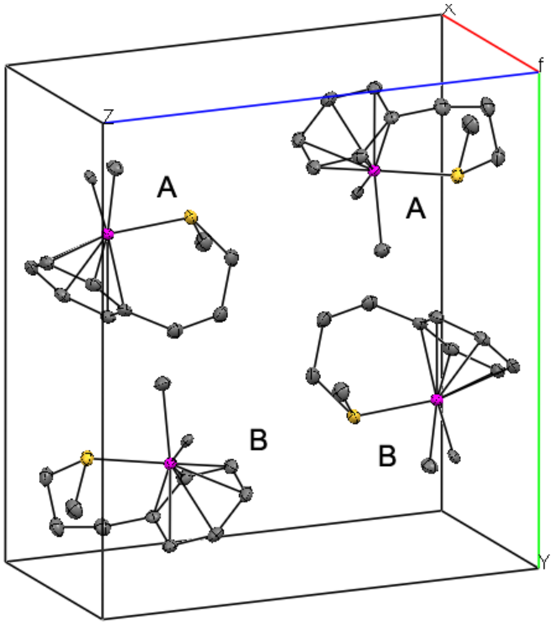

Figure S14. Unit cell for Ru$(CH_3)_2$(Ph$(CH_3)_3$$SCH_3$) **(4)** showing two different isomers A and B. Hydrogens are omitted for clarity.

Complex Ru(CH_2=CH_2)(Ph(CH_3)$_3$SCH_3) (5): Synthesis and Characterization

Scheme S5

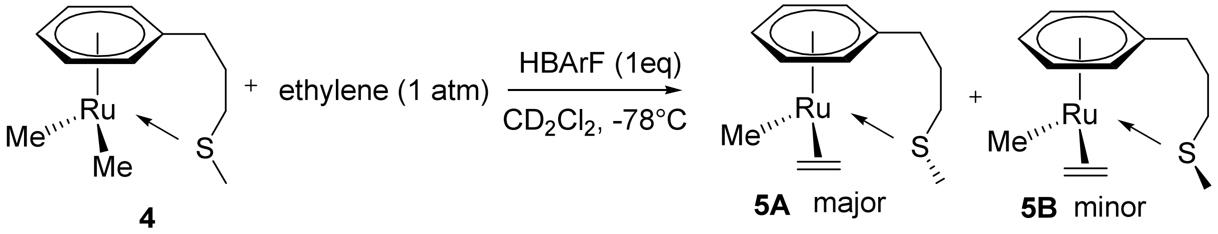

Synthesis of [Ru(η^6- Ph(CH_2)$_3$S(CH_3)$_2$(CH_2=CH_2)] (5). 0.0300 g (0.101 mmol, 1 eq) of **4** were dissolved in 1ml of CD_2Cl_2 in a NMR tube. The solution was flushed with ethylene at 1atm to saturate solution and cooled down to -78°C. ($[H(Et_2O)_2]^+$ $[BAr'_4]^-$) [1] 0.1006 g (0.101 mmol, 1 eq) were dissolved in 2ml of CD_2Cl_2. Addition of ($[H(Et_2O)_2]^+$ $[BAr'_4]^-$) solution was added through needle to complex **4** solution at -78°C. This solution is used for complex characterization and insertion studies. Two isomers are formed as depicted on the scheme above, reported only the peaks for the major compound. Poor stability forbids complex isolation and needs to be prepared in-situ for NMR or polymerization studies. NMR (500 MHz, CD_2Cl_2, 183K): δ 6.08 (dd, 5.5, 5.5 Hz, 1H), 6.00 (d, 5.5 Hz, 1H), 5.74 (d, 5.5 Hz, 1H), 5.51 (dd, 5.5, 5.5 Hz, 1H), 4.78 (dd, 5.5, 5.5 Hz, 1H), 3.89 (m, 1H), 3.14 (d, 6.0 Hz, 1H), 2.76 (dd, 5.5, 12.5 Hz 1H), 2.36-1.72 (m, 7H), 1.83 (s, 3H). ^{13}C NMR (500 MHz, $CDCl_3$, 183K): δ157.6, 105.7, 100.7, 93.9, 89.1, 86.8, 53.6, 31.8, 29.5, 20.8, 20.5, -10.1. HRMS (ESI+, CH_2Cl_2) *m/z* calcd for $C_{15}H_{26}SRu$ $[M]^+$, 339.5; found $[M]^+$, 339.07.

MNR and MS studies on Complex Ru(CH_2=CH_2)(Ph(CH_3)$_3$SCH_3) (5).

Figures S15-S21 display 1H-NMR, 13C-NMR, HMQC, COSY, and NOE experiments for complex **5**. As can be seen two different species can be identified. Complex **5A** (Scheme S5) is the more abundant due to less steric interaction with S-Me moety. Major compound can be clearly identified although overlapping of peaks forbids complete assignment of the tethered arm protons. Aromatics can be assigned unambiguously as well as methyl-thiol and ruthenium-methyl peaks. Arene area smaller peaks due to the minor compound can also be assigned. By integration at 183K compound **5A** is more abundant in a 4:1 ratio.

Figures S22 and S23 depict the stacking of proton NMRs at different temperatures. At low temperatures coordinated ethylene does not have free rotation therefore four different proton and two carbon signals can be assigned. Unfortunately overlapping with ether peaks makes the peak assignment of ethylene difficult at 183K. Increasing temperature makes ethylene peaks coalesce at 2.90 ppm due to ethylene rotation. At higher temperature (263K, figures S24-S27) the species ratio is 2:1 and at 298K the presence of both species makes peaks broader and hard to identify (figure S23) only coordinated ethylene and ruthenium-methyl peak are distinguishable. Additional NMR experiments were run at 263K (figures S24-S27) and allow to better assign the peaks corresponding to coordinated ethylene with free rotation. Integration of ethylene peaks is 6 protons which confirms the presence of two isomer in a 2:1 ratio.

Heating sample at 318 K and holding temperature for 15 minutes allows for the observation of ethylene consumption and disappearance of Ru-Me signal which is indicative of migratory insertion (figure S28).

Mass Spectrometry analysis of the NMR tube heated up to 318 K for 15 minutes (figures S29-S32) confirms the presence of several oligomeric species growing on the ruthenium metal, which explains the complication of the NMR spectra. A series of growing species (oligomers) were observed with various numbers of ethylene insertion (n=1,3,5,7 figure S29, red dots) as a result of direct ethylene insertion. Also growing species as a result β-Hydrogen elimination and chain transfer followed by ethylene coordination and insertion can be observed (n=0,2,4,6 figure S29, blue dots).

Isotopic modeling of each of these species and compared to experimental results confirm their identity (figures S30 and S31). Similar MS spectra when complex **3** is activated with $AlMe_2Cl$ in the presence of ethylene above 318.15 K (Figure S32).

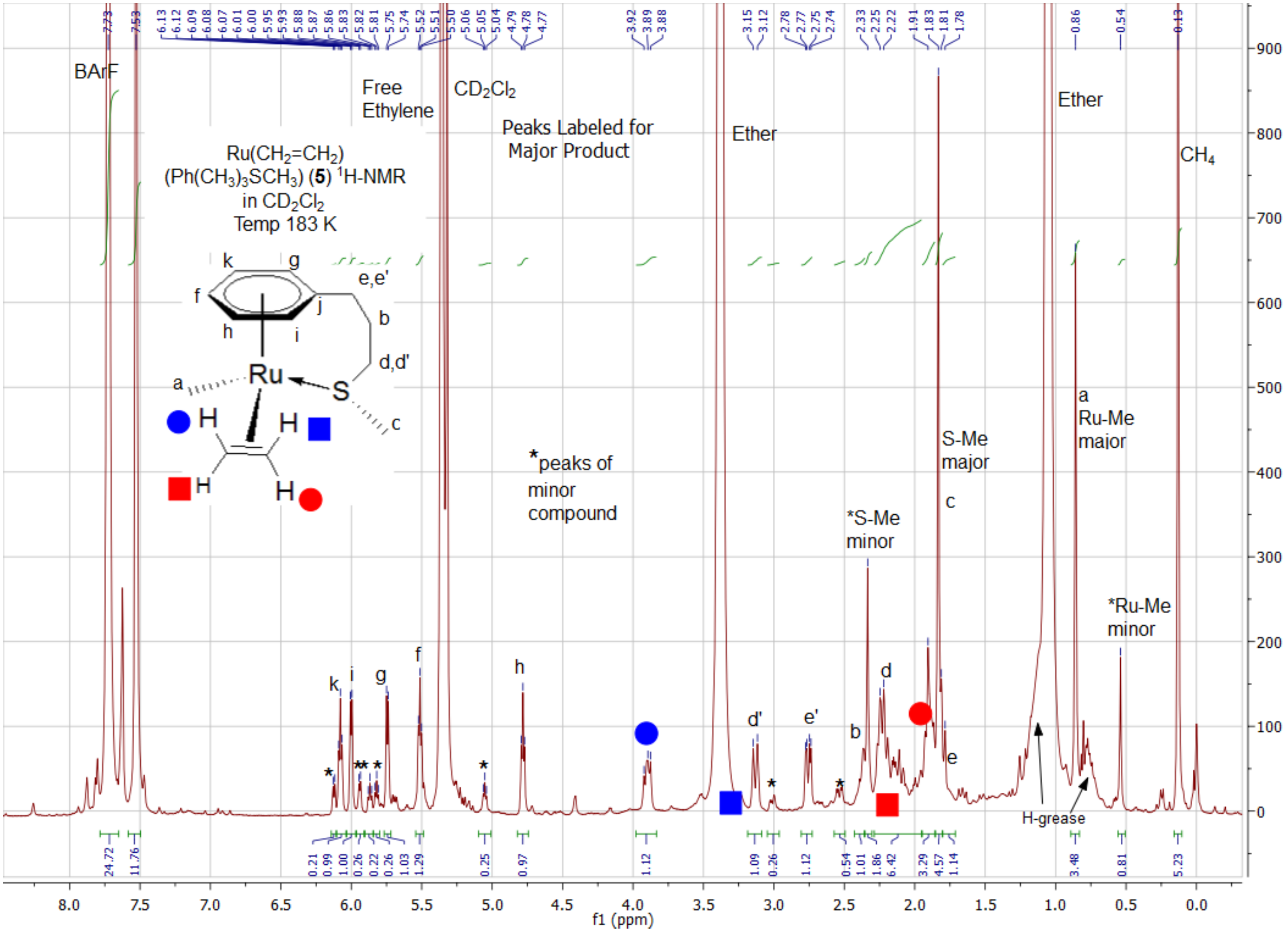

Figure S15. ^{1}H-NMR spectrum of complex **5** at 183 K in CD_2Cl_2.

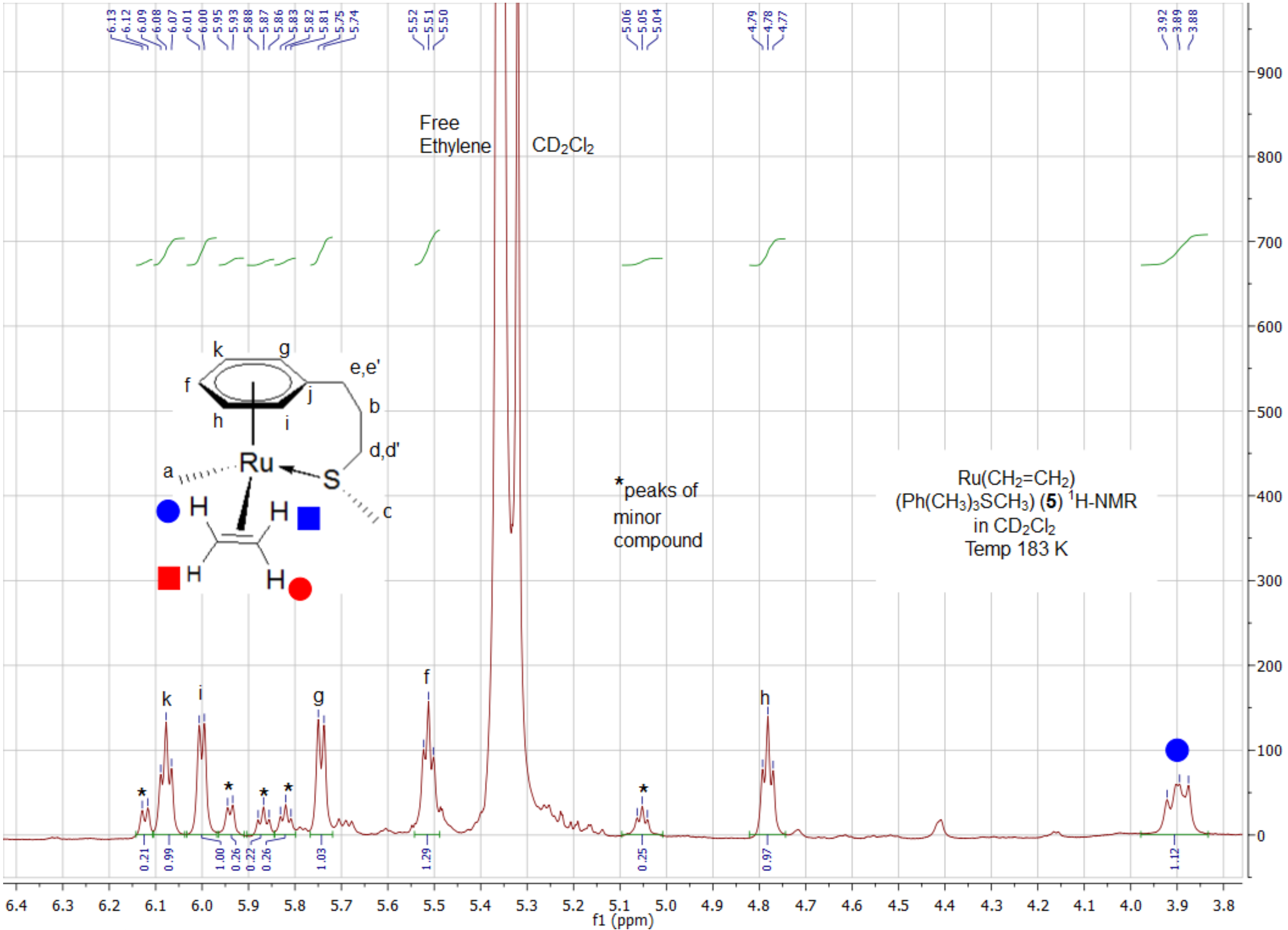

Figure S16. ^{1}H-NMR spectrum of complex **5** (with aromatic region expanded) at 183 K in CD_2Cl_2.

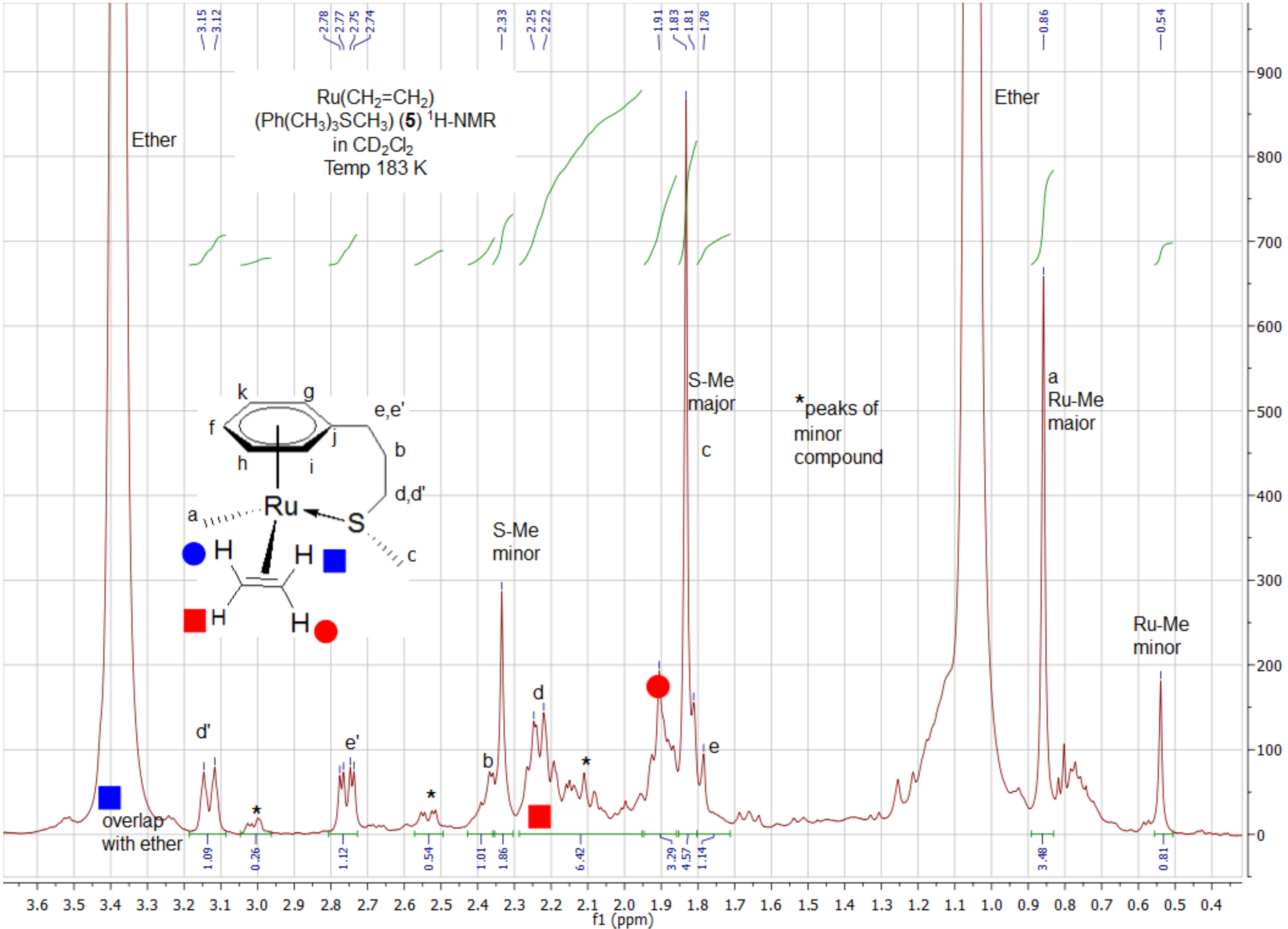

Figure S17. ^{1}H-NMR spectrum of complex **5** (with aliphatic region expanded) at 183 K in CD$_2$Cl$_2$.

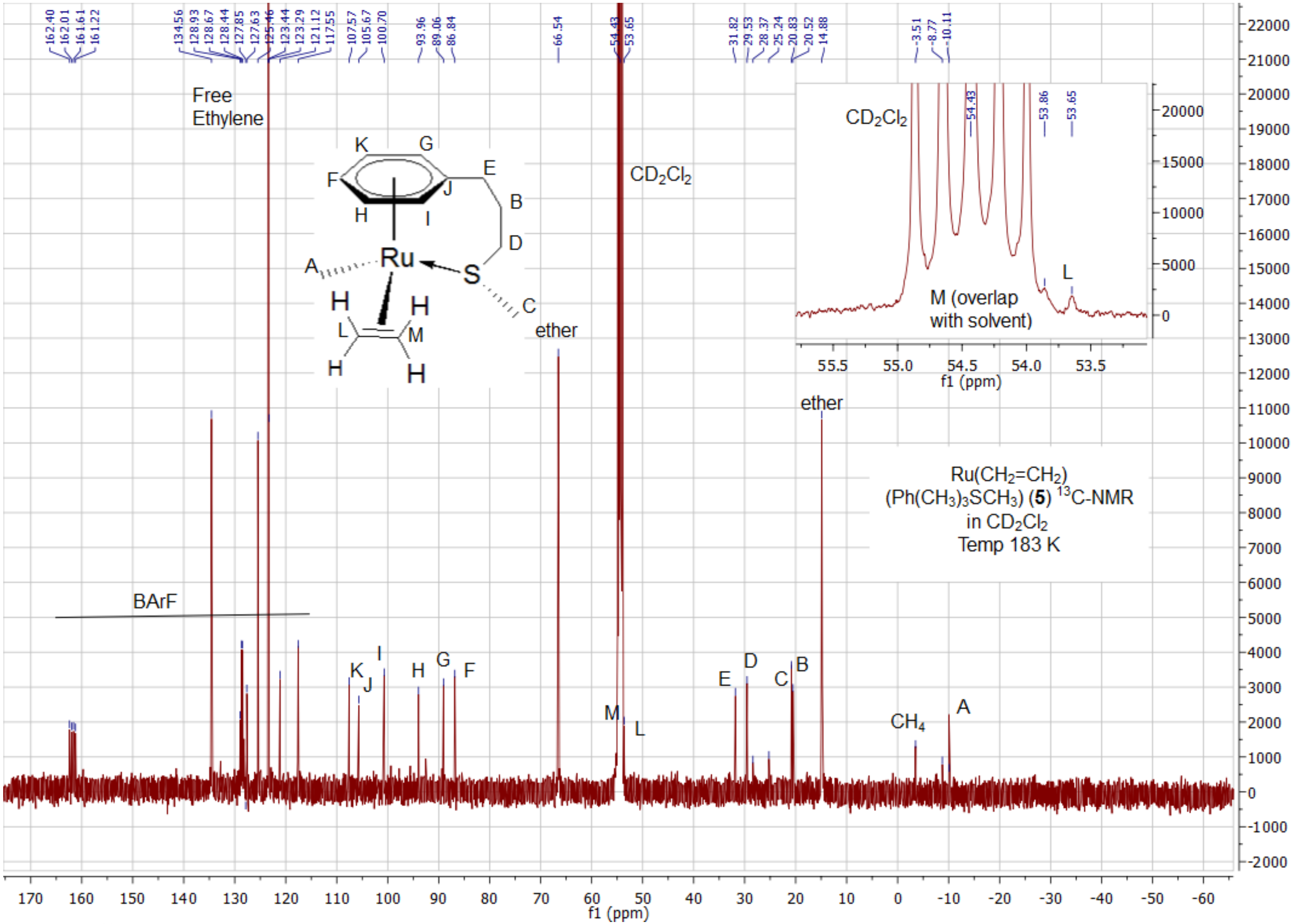

Figure S18. ^{13}C-NMR spectrum of complex **5** at 183 K in CD_2Cl_2.

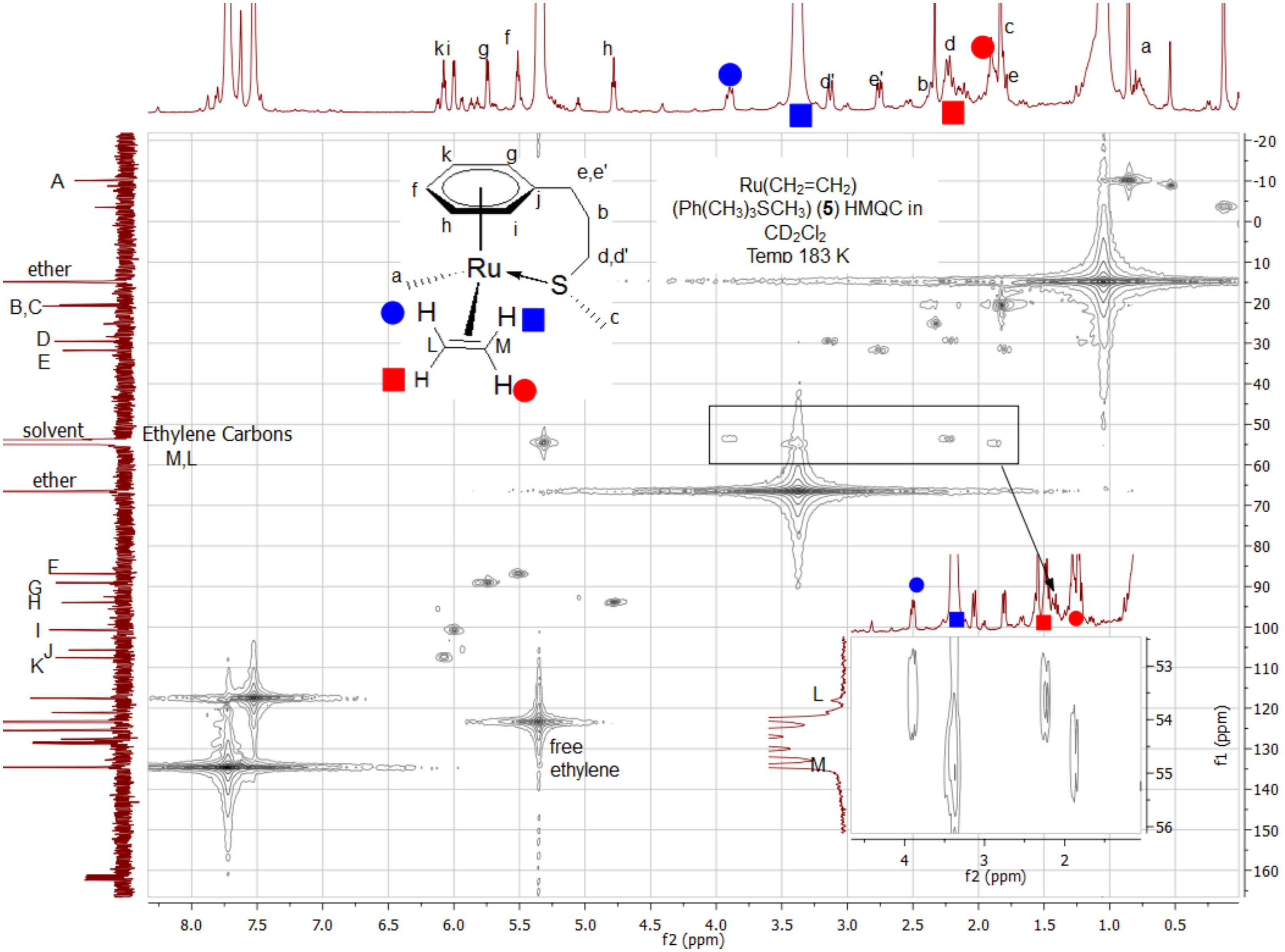

Figure S19. HMQC-NMR spectrum of complex **5** at 183 K in CD_2Cl_2.

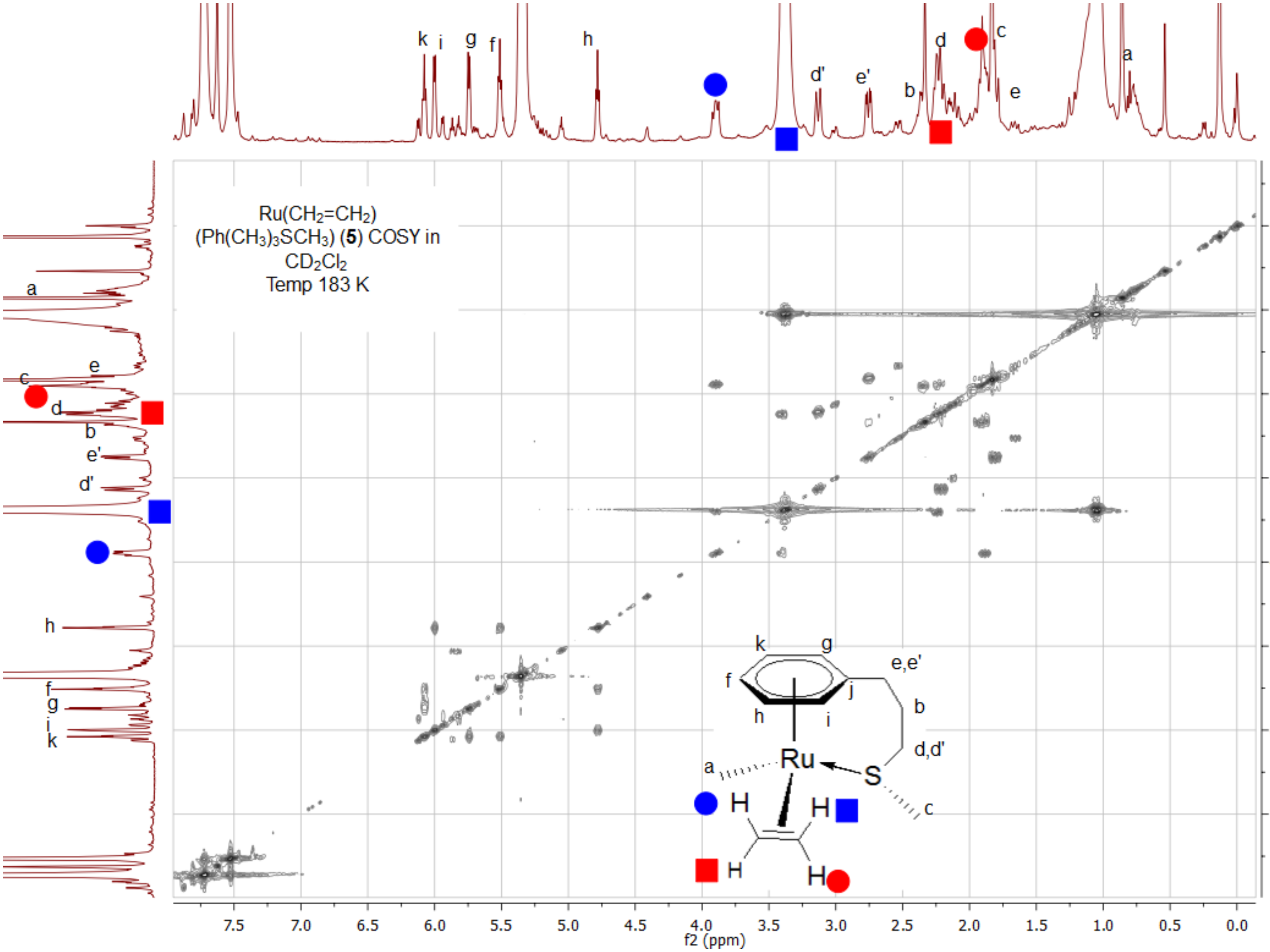

Figure S20. COSY-NMR spectrum of complex **5** at 183 K in CD_2Cl_2.

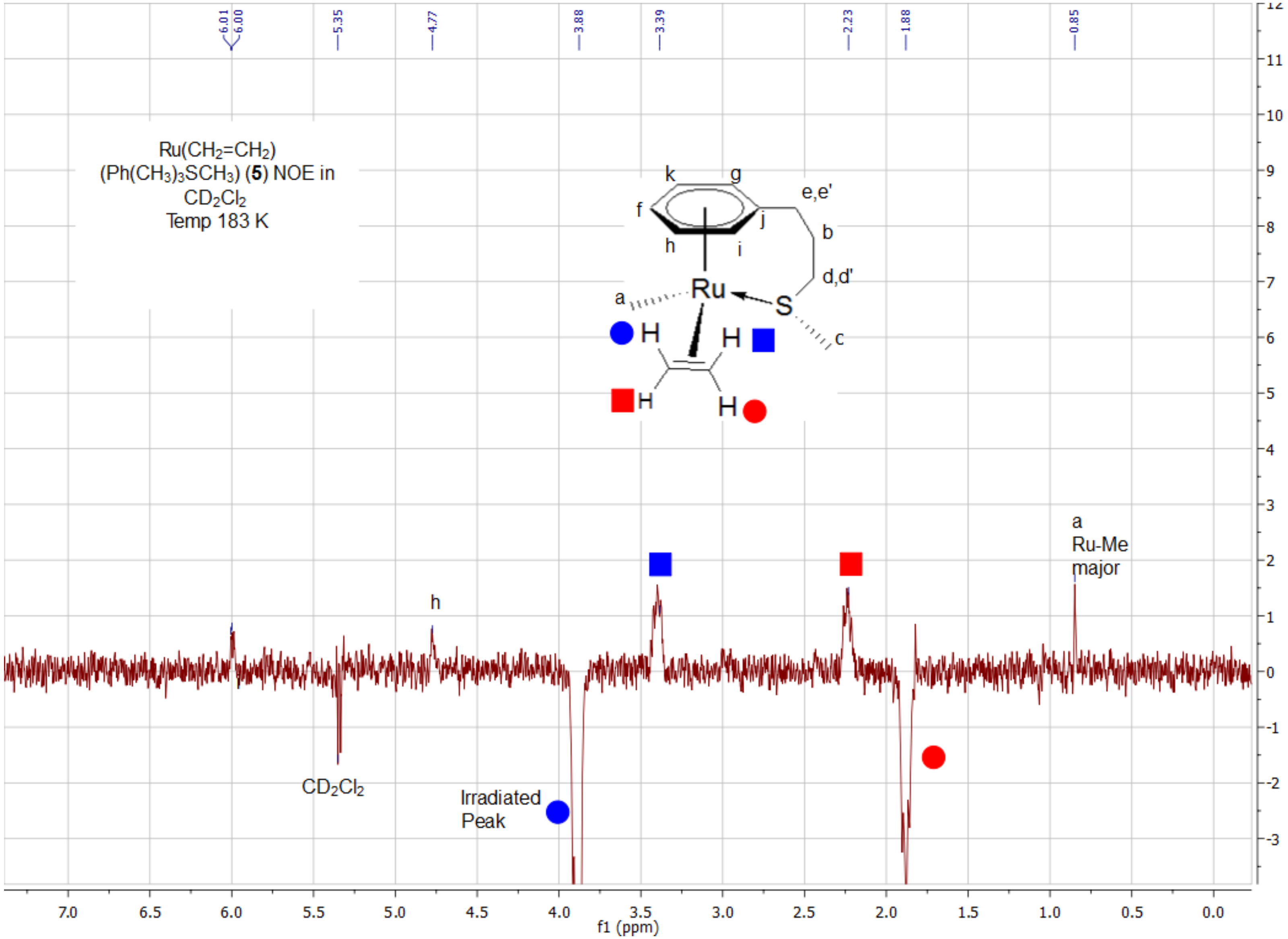

Figure S21. NOE-NMR spectrum of complex **5** at 183 K in CD_2Cl_2.

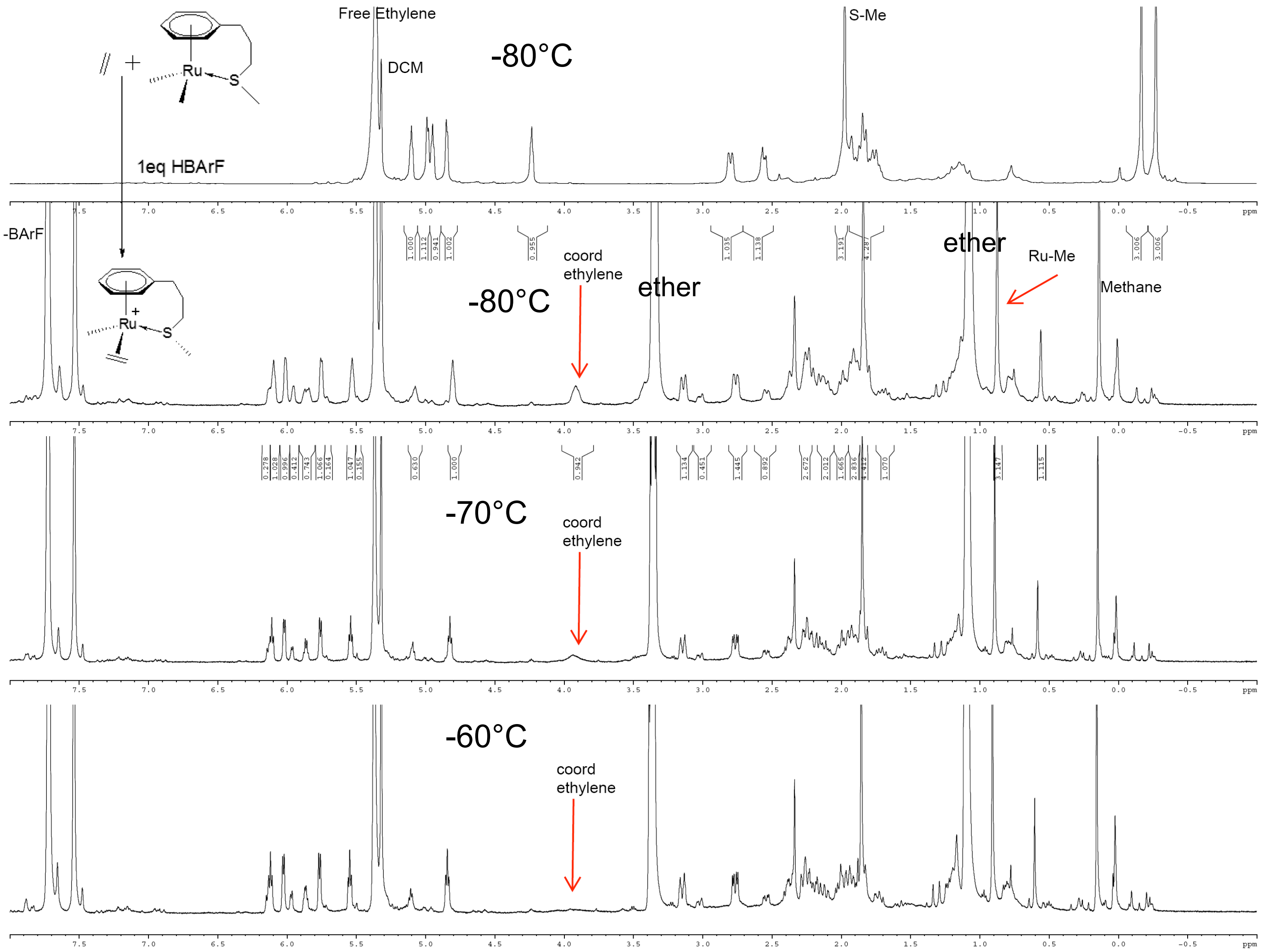

Figure S22. Variable temperature (193-213K) ^{1}H-NMR spectrum of complex **5** in CD_2Cl_2.

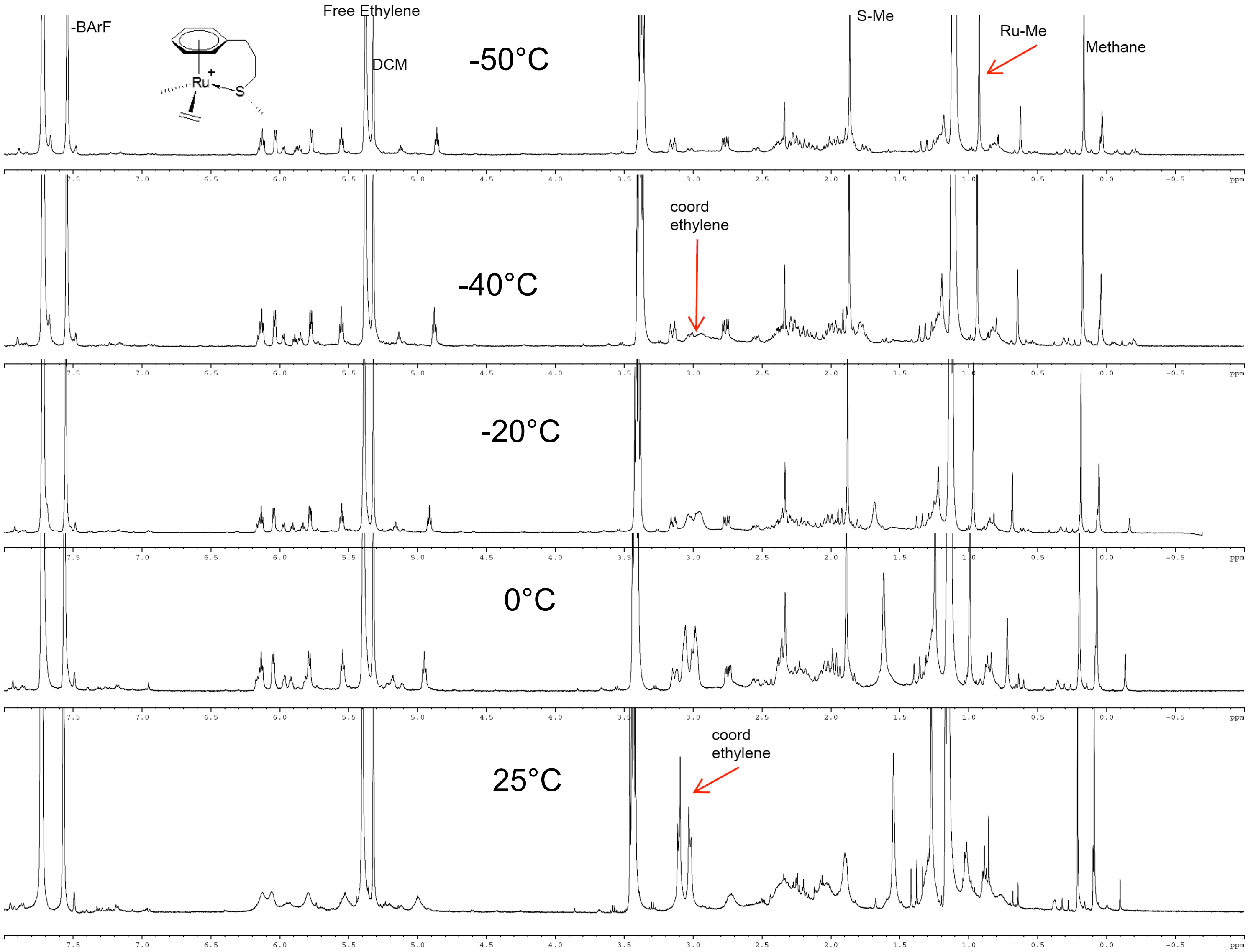

Figure S23. Variable temperature (223-298K) ^{1}H-NMR spectrum of complex **5** in CD_2Cl_2.

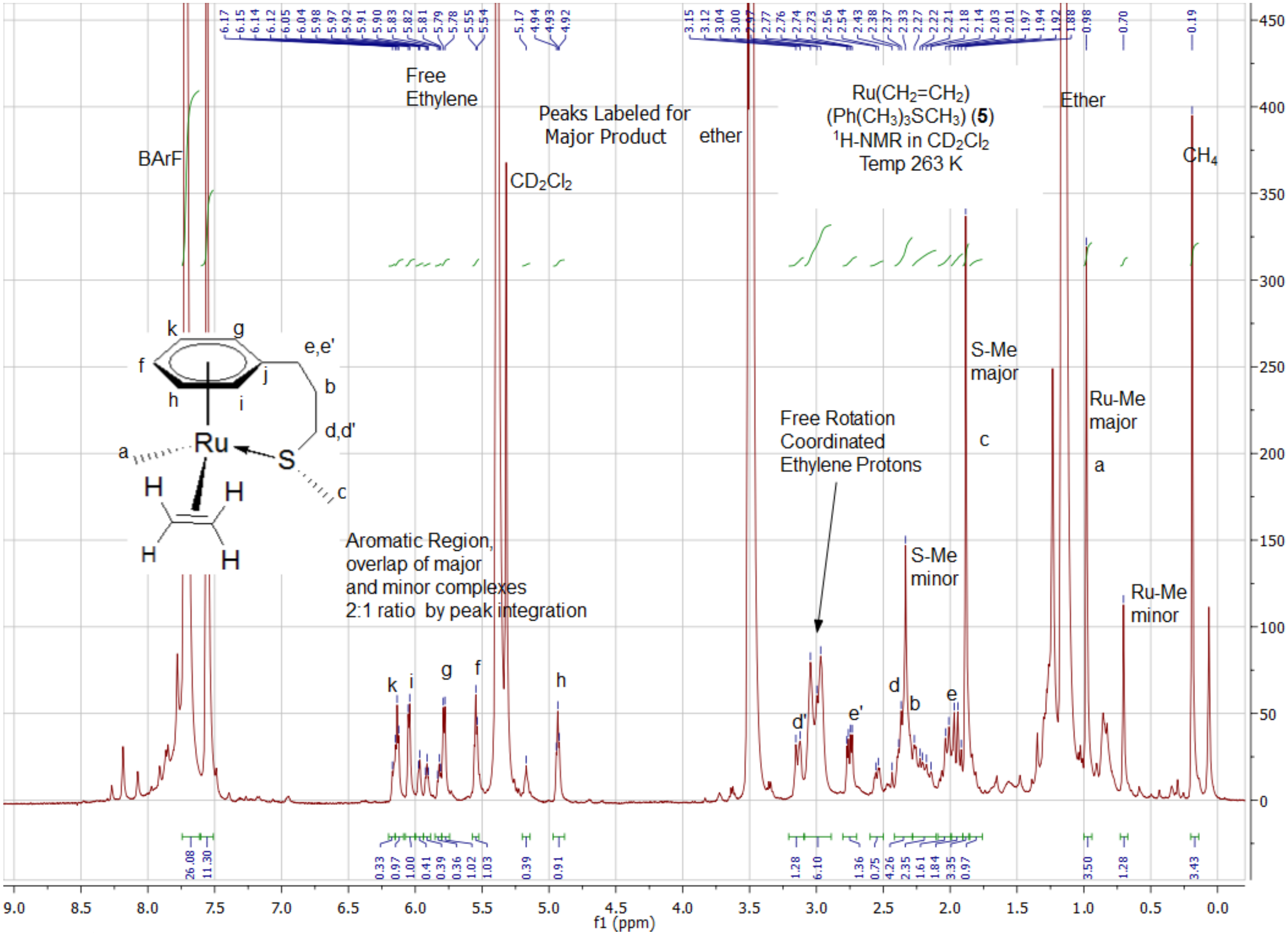

Figure S24. ^{1}H-NMR spectrum of complex **5** at 263 K in CD_2Cl_2

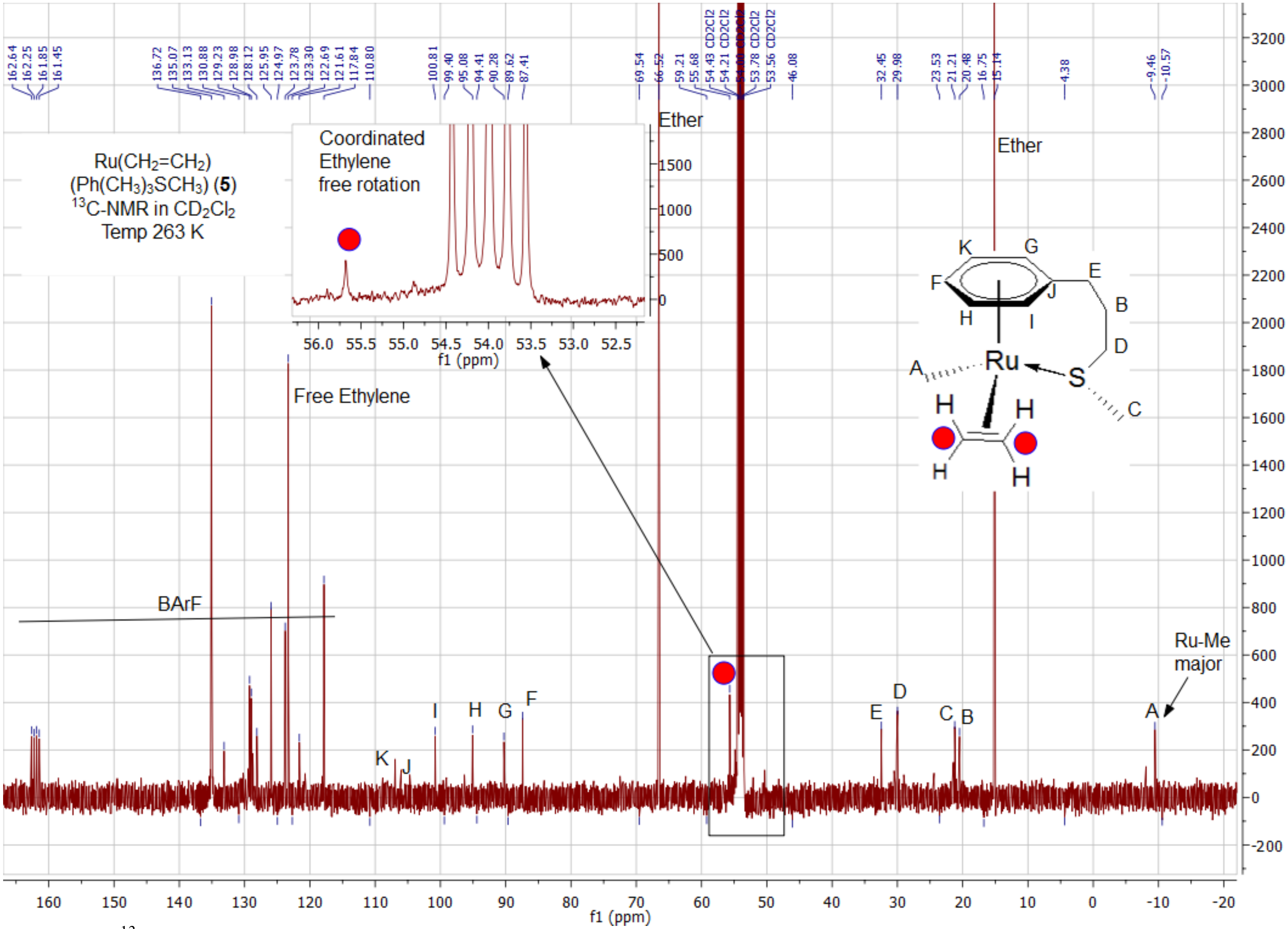

Figure S25. ^{13}C-NMR spectrum of complex **5** 263 K in CD_2Cl_2.

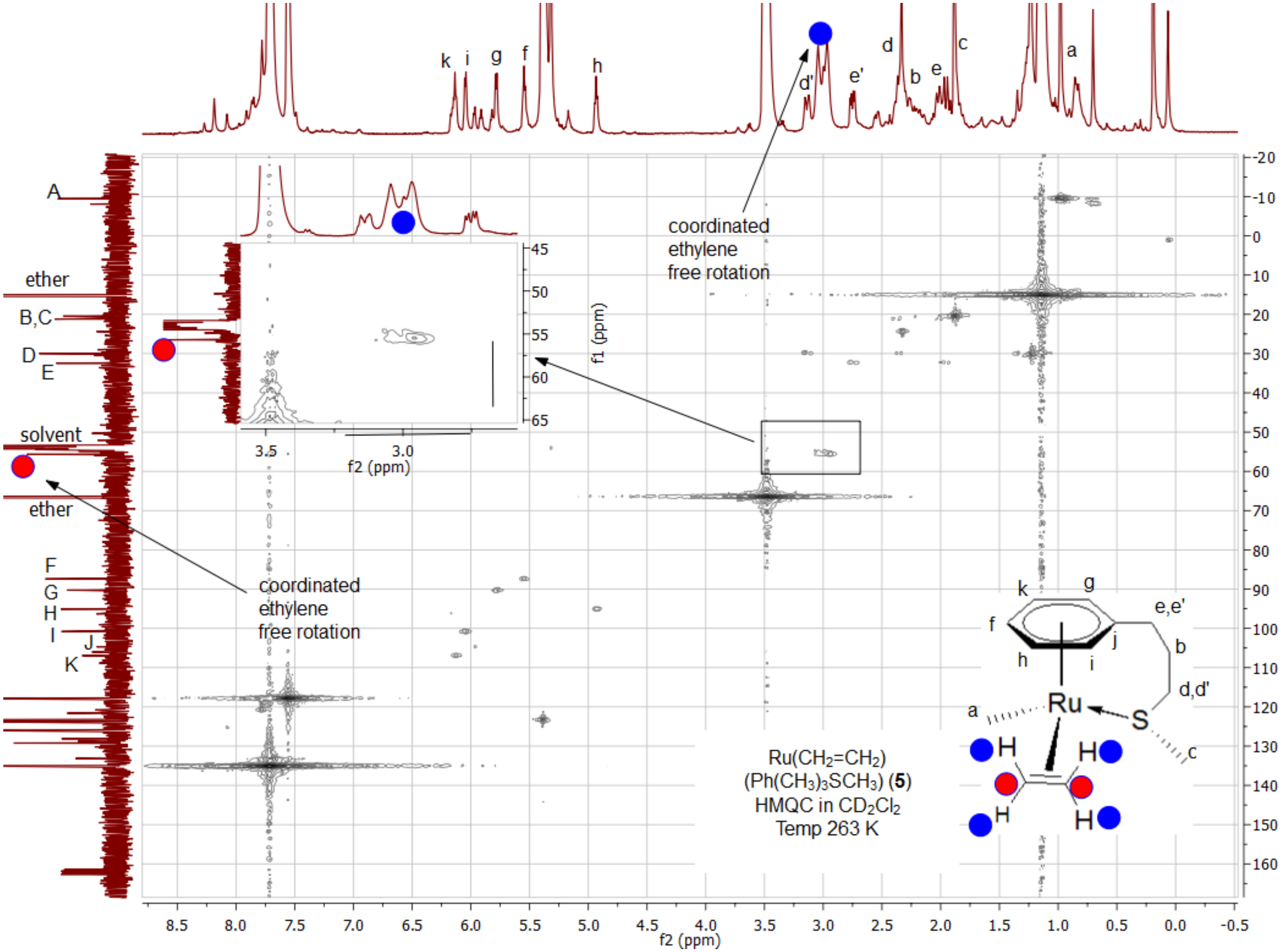

Figure S26. HMQC-NMR spectrum of complex **5** at 263 K in CD_2Cl_2.

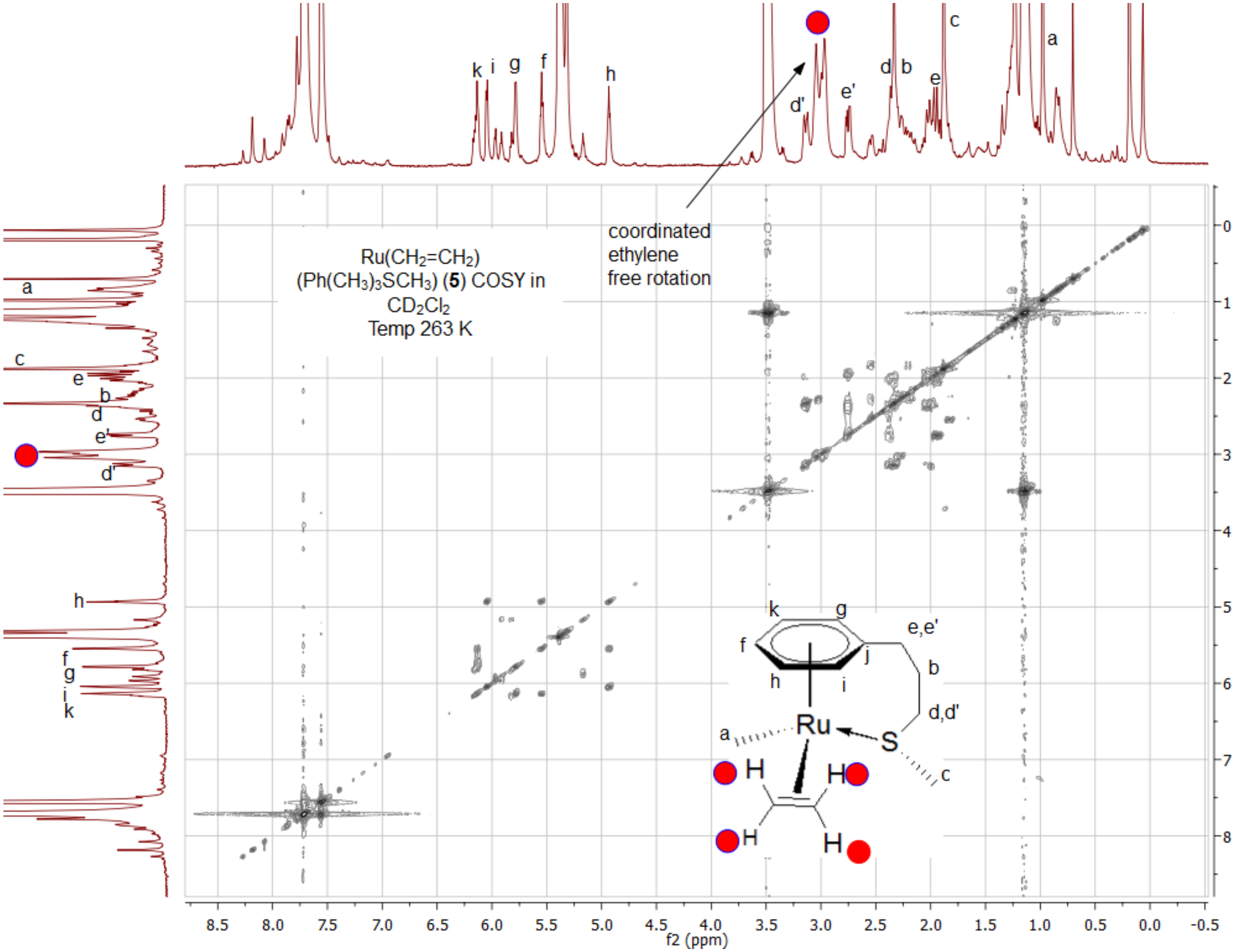

Figure S27. COSY-NMR spectrum of complex **5** at 263 K in CD_2Cl_2.

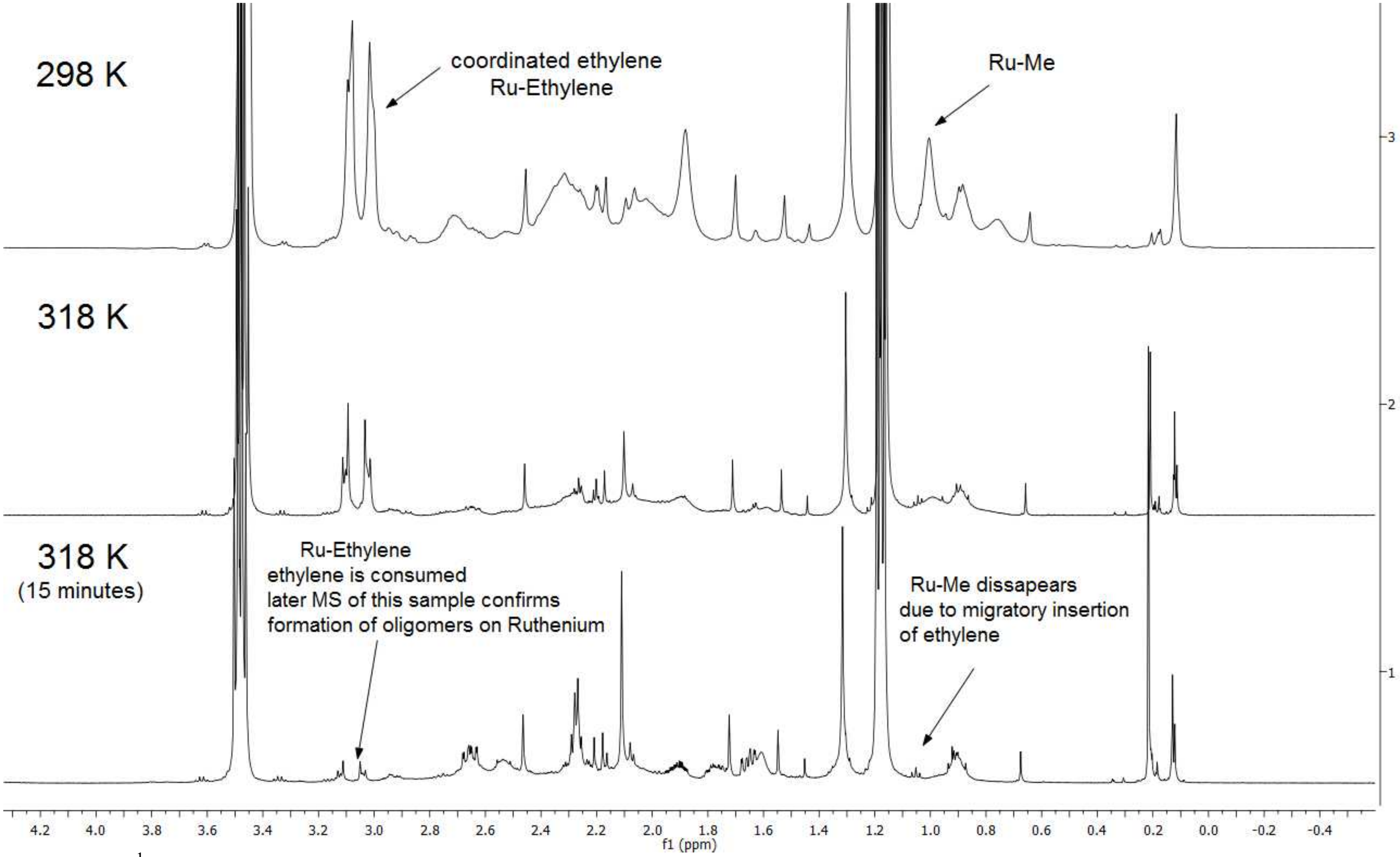

Figure S28. ^{1}H-NMR spectra of complex **5** running at different temperature (in CD_2Cl_2 from 298 K to 318 K, and then hold at 318 K for 15 minutes). Ethylene consumption and Ru-Me peak disappearance provide direct evidence for ethylene migratory insertion on Ru center. ESI-MS spectrum in the subsequent figure is from this sample probing growing oligomers bound on Ru center.

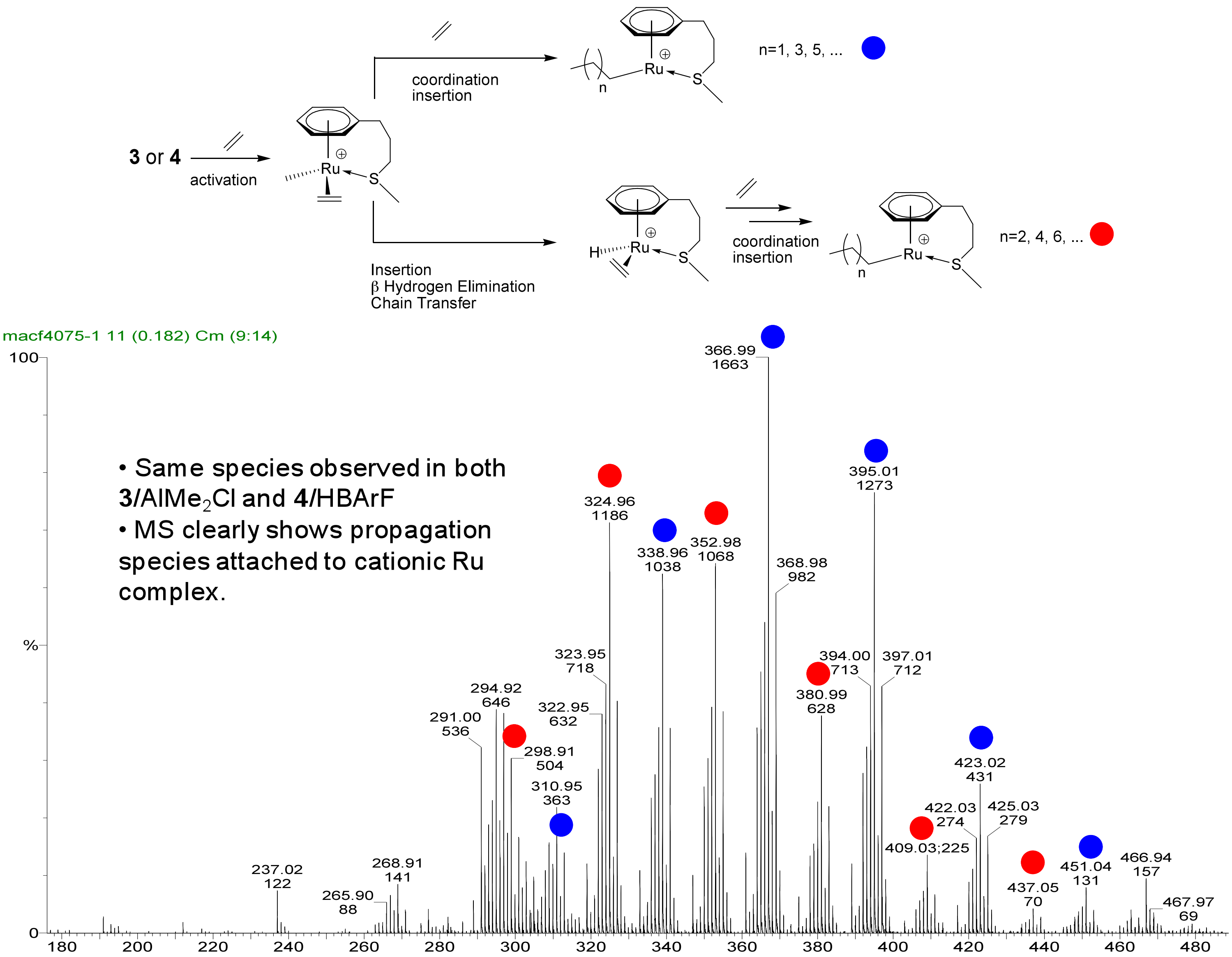

- Same species observed in both $3/AlMe_2Cl$ and $4/HBArF$
- MS clearly shows propagation species attached to cationic Ru complex.

Figure S29. ESI-MS spectrum of ethylene oligomer species formed *in situ* with **4**/($[H(Et_2O)_2]^+$ $[BAr'_4]^-$).

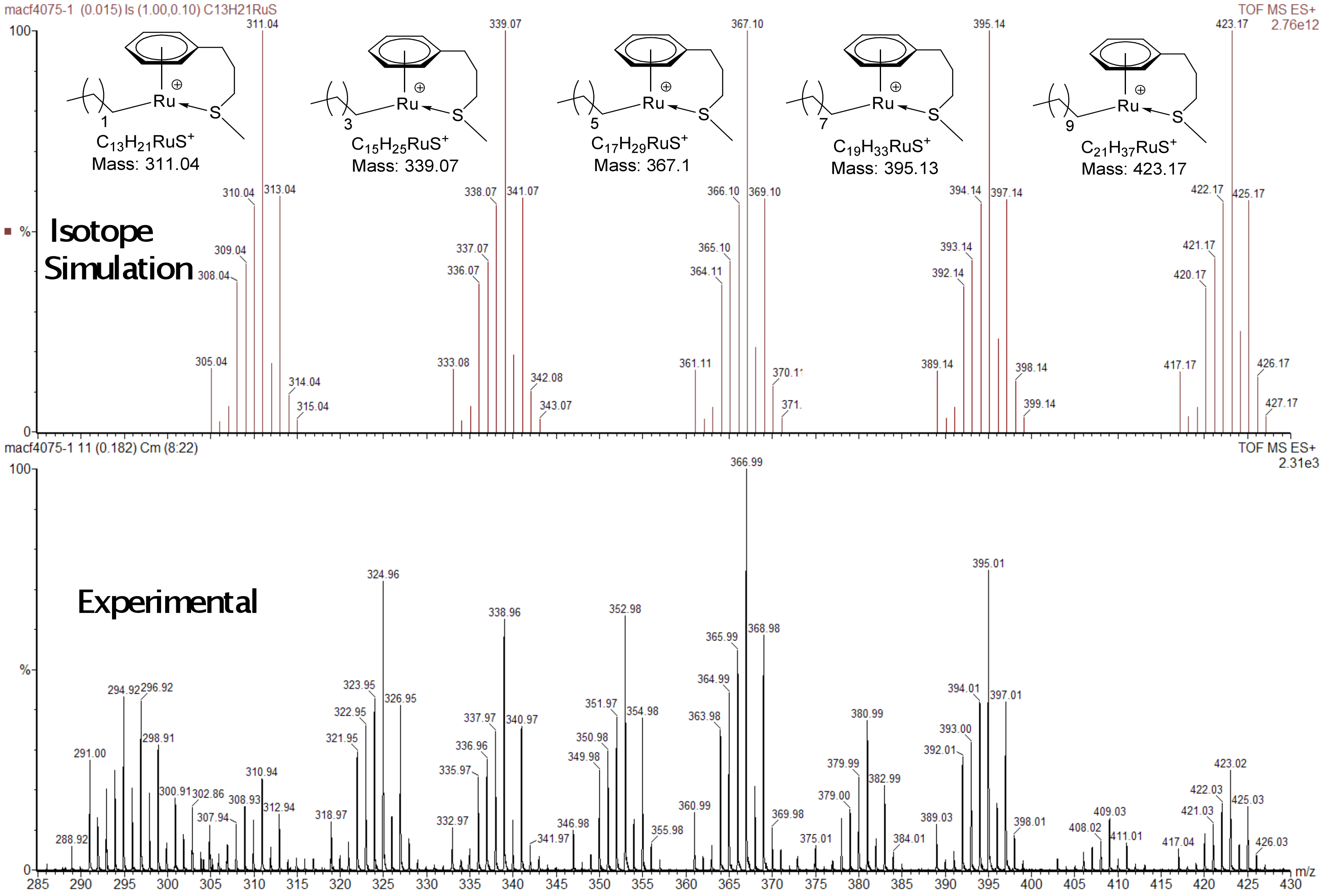

Figure S30. ESI-MS of ethylene oligomers bound to cationic Ru center formed by primary ethylene insertion (oligomers with odd number of carbons). Comparison between isotope modeling (top) and experimental data (bottom).

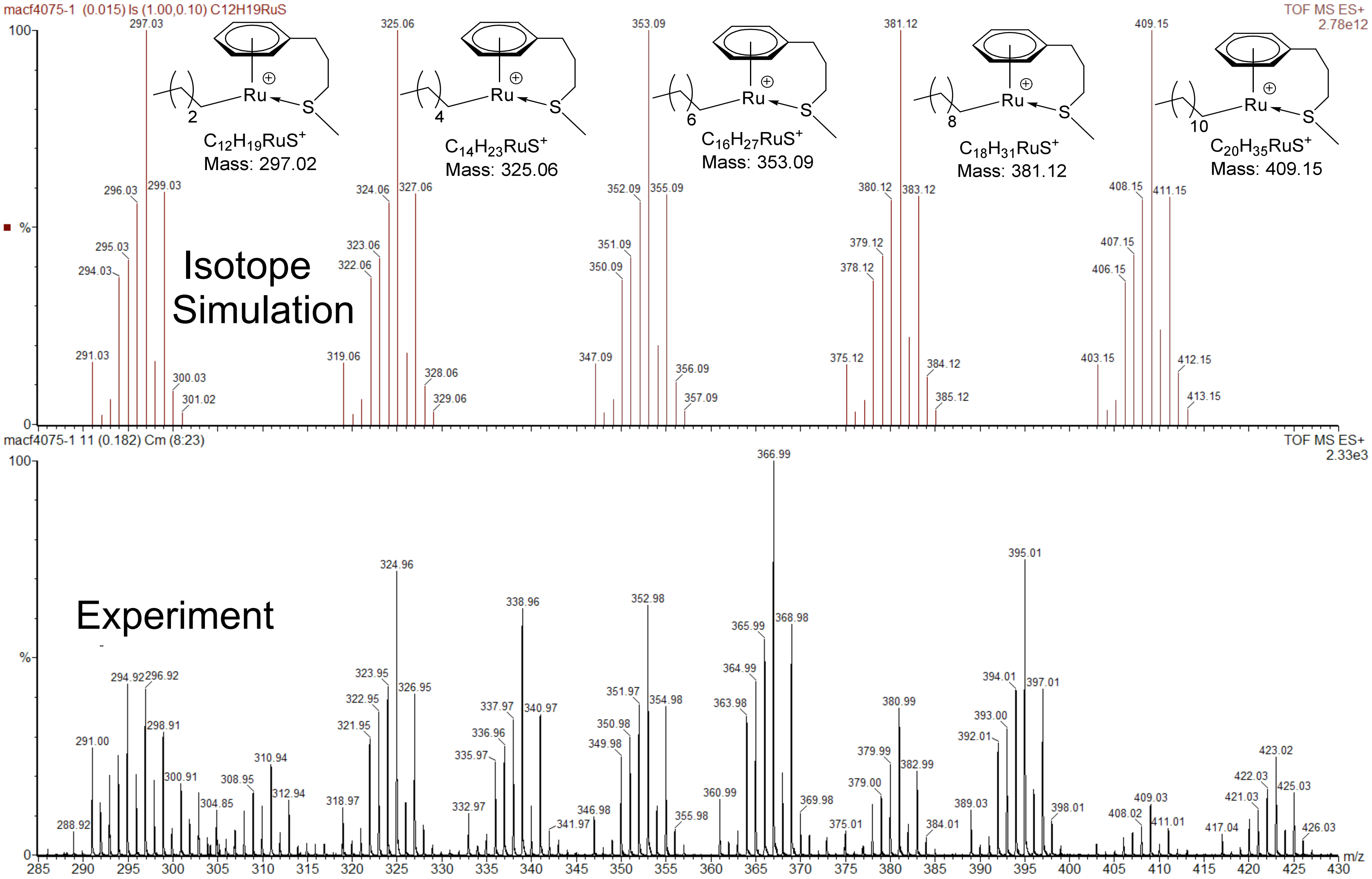

Figure S31. ESI-MS of ethylene oligomers bound to cationic Ru center formed by ethylene insertion after chain transfer (oligomers with even number of carbons). Comparison between isotope modeling (top) and experimental data (bottom).

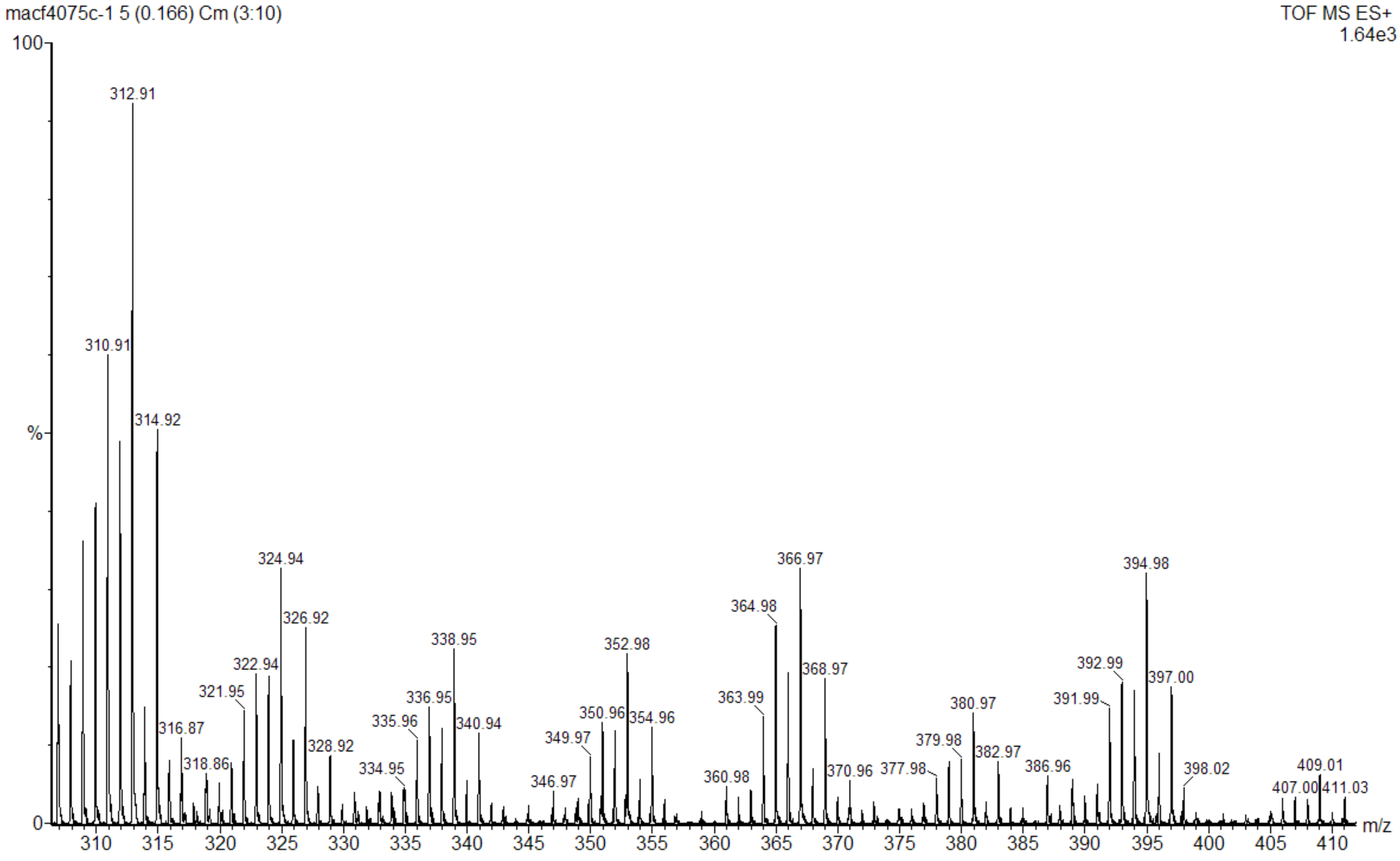

Figure S32. ESI-MS spectrum of ethylene oligomers bound to cationic Ru center formed *in situ* with **3**/$AlMe_2Cl$ system.

Insertion barrier calculation and ethylene consumption monitoring.

Complex **5** (mixture of isomers **5a** and **5b**) was prepared as previously described (*vide supra*) in order to study insertion barriers. Complex **5** was warmed from 183 K to 273 K and then warmed stepwise in 2.5 degree increment. First insertion was clearly observed seen at 288 K by the appearance of a shoulder after 1 hour overlapping with the **5a** Ru-Me peak (Fig. S33). Increasing temperature to 301 K resulted in faster insertion (Fig. S33 and S34), allowing for kinetic study in a timely manner. The Ru-Me peak for **5a** significantly overlaps with growing oligomers and polymer chains (Fig. S34), which precluded quantitative kinetic analysis. The Ru-Me peak for the minor isomer, **5b**, is separated from other peaks, and was used for determining the initial migratory insertion barrier (Fig. S33 & S34). The disappearance of this methyl peak was monitored at 301 K for 7 hr, and initial migratory insertion barrier was calculated following the Brookhart's report.[12] The Ru-Me peak disappearance for **5b** follows a first-order kinetics (Fig. S35) with a rate constant $k = 1.9\text{x}10^{-4}\ \text{s}^{-1}$ at 301 K. The calculated initial migratory insertion barrier (301 K) was $\Delta G^{\ddagger} = 22.8 \pm 0.1$ kcal/mol (**5b**). Ethylene consumption was also monitored (Fig. S36 and S37) with time, which correlates well with Ru-Me disappearance. Figure S36 depicts graphically this correlation. Figure S37 displays the plot of integral change overtime comparing free ethylene consumption and Ru-Me (**5b**) disappearance. (Free ethylene peak has some minor overlap with aromatic protons from the ligand, integral were estimated by comparison with the coordinated ethylene peaks). We cannot distinguish ethylene consumption from **5a** or **5b** complexes, nevertheless there is a clear correlation between ethylene consumption and Ru-Me disappearance. Chain growth and resonance of the oligomers was impossible to determine due to peaks overlap.

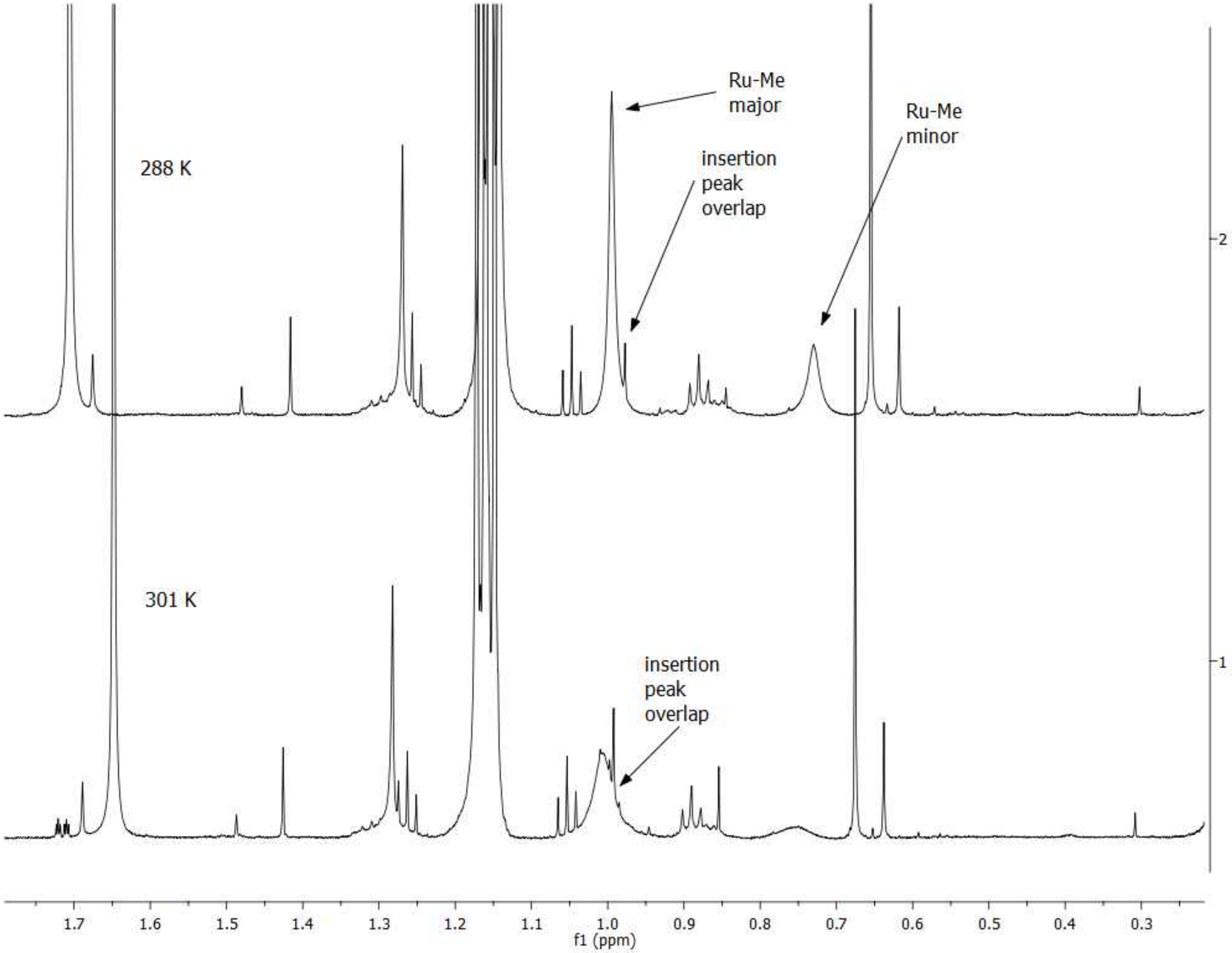

Figure S33. Monitoring Ru-Me peak for complexes **5a** and **5b**. First insertion is observed at 288 K. Peaks overlaps of the major isomer (**5a**) prevents quantitative kinetic analysis; therefore, we used minor isomer peak (**5b**) for kinetic treatments. Increasing temperature to 301 K leads to faster insertion, despite some peak broadening.

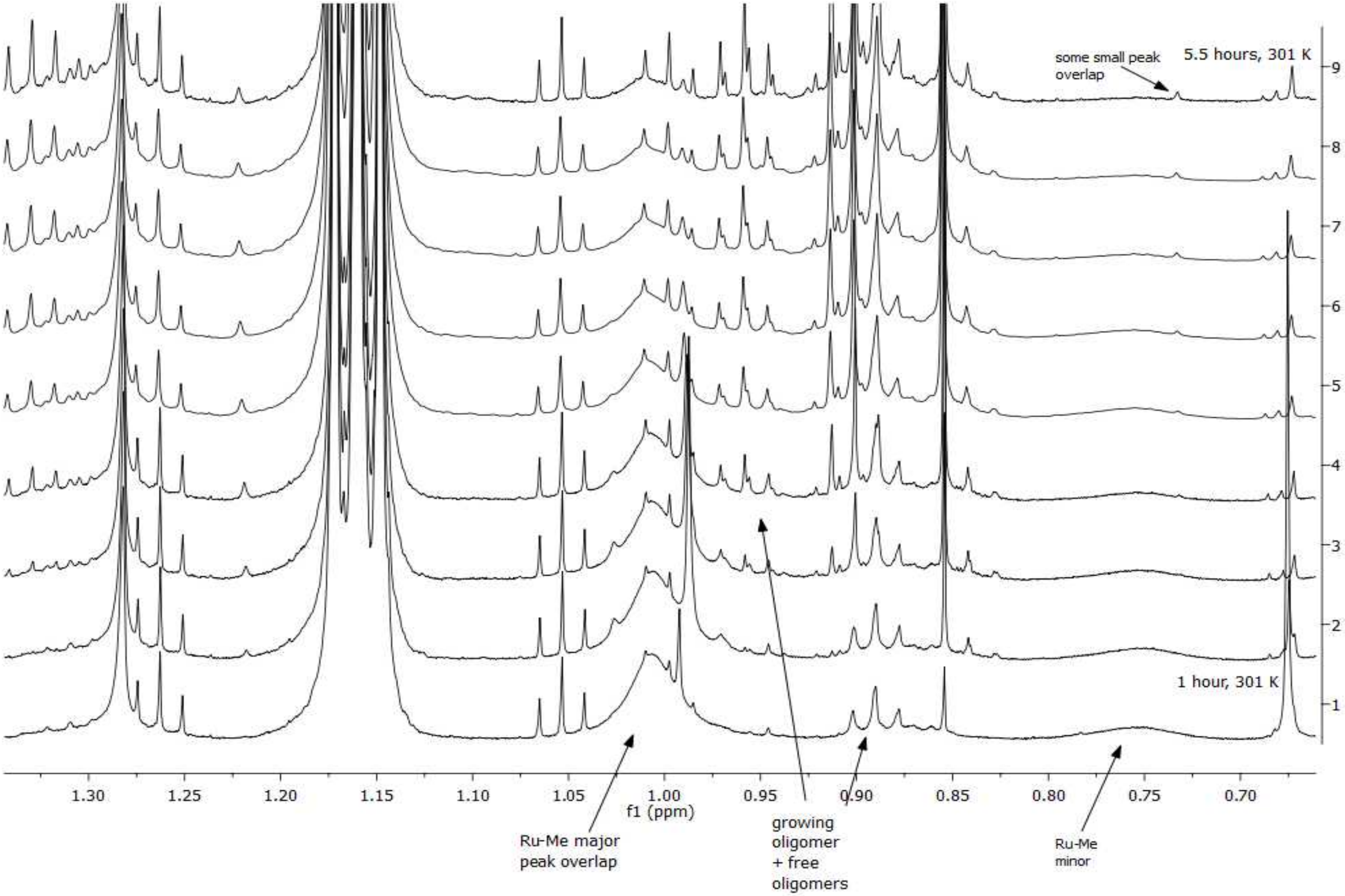

Figure S34. Monitoring of Ru-Me disappearance for complex **5b**.

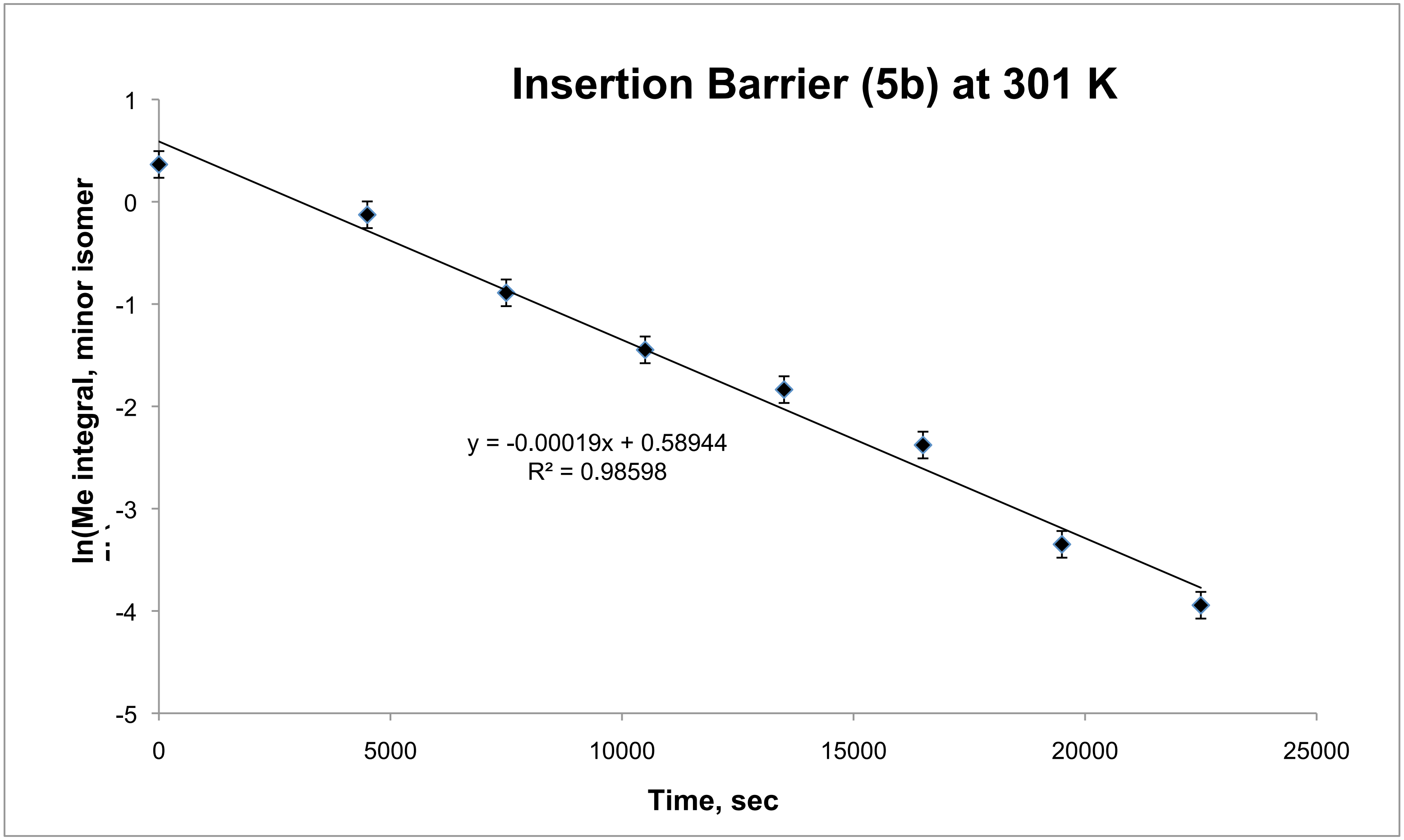

Figure S35. First-order kinetic plot for Ru-Me disappearance (**5b**) at 301 K.

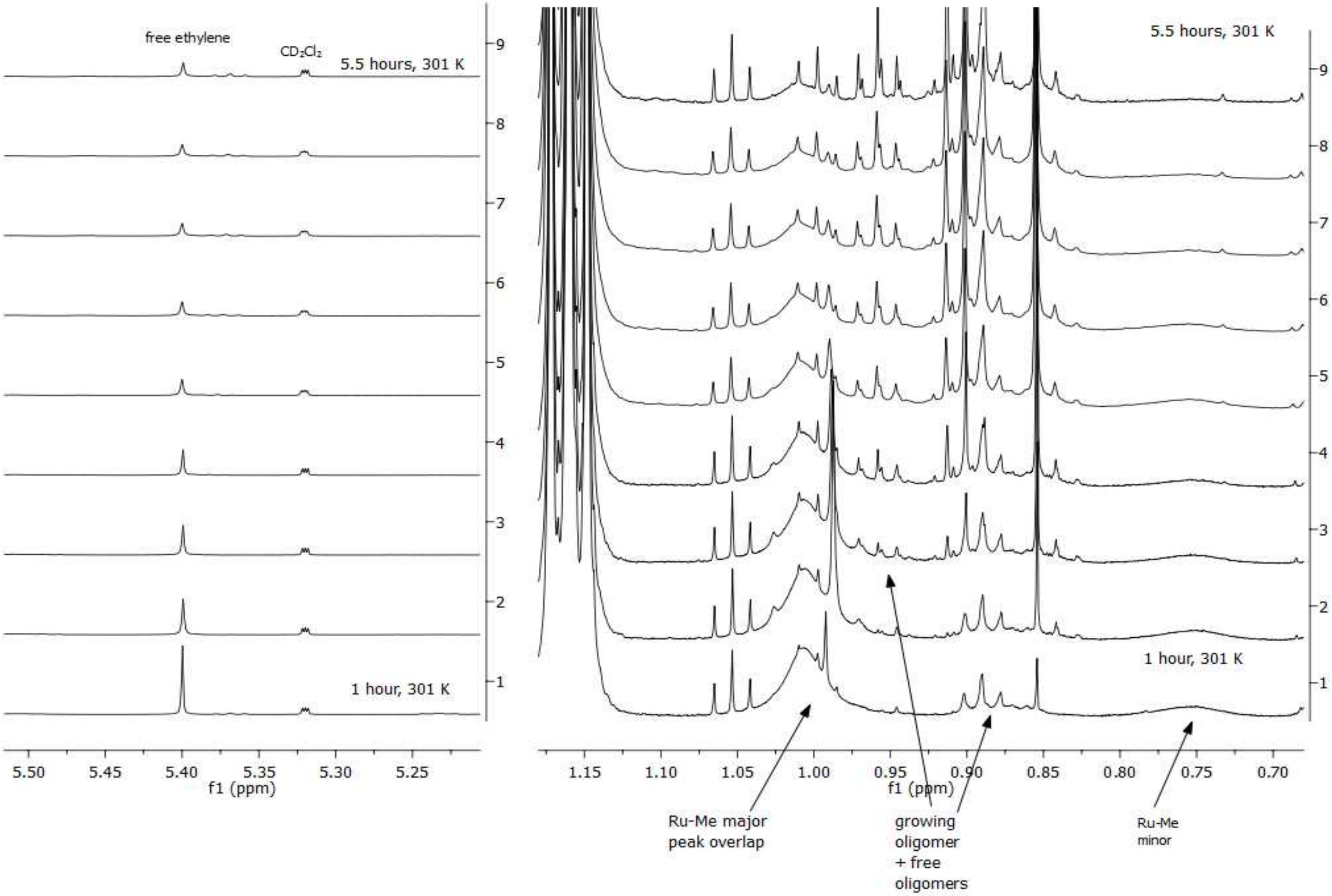

Figure S36. Monitoring free ethylene consumption and Ru-Me peak disappearance for complex **5**. It should be noted that ethylene was consumed by both isomers **5a** and **5b**.

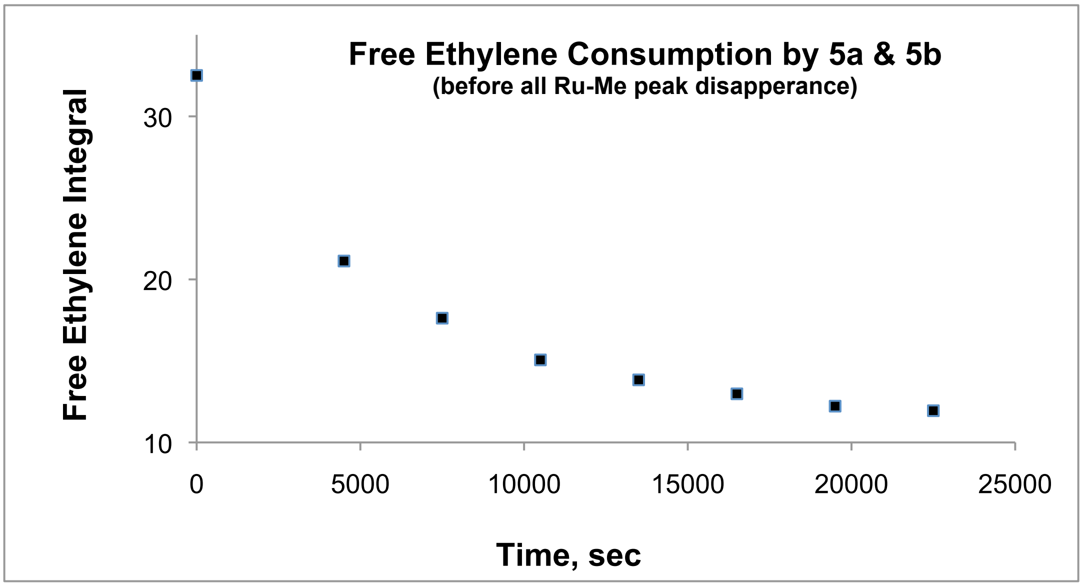

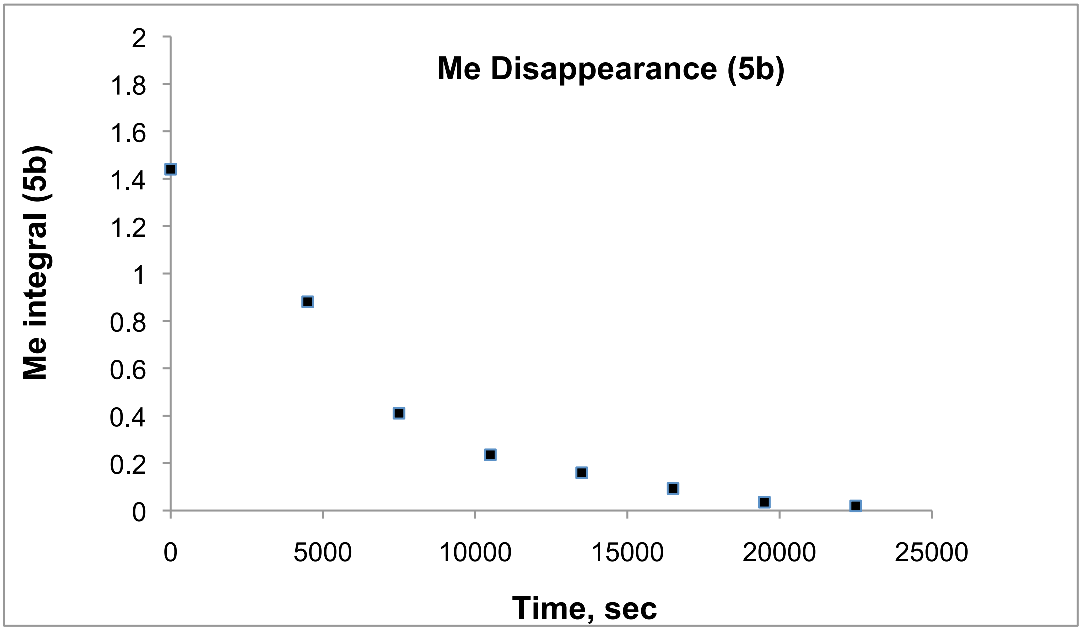

Figure 37. Top: ethylene consumption by complex **5** (**5a** and **5b**) monitored at 301 K. Bottom: Ru-Me disappearance for **5b** monitored at 301 K.

^{1}H-NMR Polymer Characterization, Differential Scanning Calorimetry (DSC), and Gel Permeation Chromatography (GPC)

Figure S38 is the characteristic proton NMR of polyethylene oligomers obtained with complex **4** upon activation with ($[H(Et_2O)_2]^+$ $[BAr'_4]^-$). The set of peaks at 5.4 clearly show the formation of internal olefin which is characteristic isomerization by the metal complex.

Figure S39 is the characteristic DSC obtained for polyethylene from polymerization of complex **4** upon activation of ($[H(Et_2O)_2]^+$ $[BAr'_4]^-$). Low melting temperature (Tm) indicates the formation of low molecular weight polyethylene.

Figures S40 and S41 display characteristic GPC data of polymers made with **3**/$AlMe_2Cl$ and **4**/$[H(Et_2O)_2]^+$ $[BAr'_4]^-$ respectively.

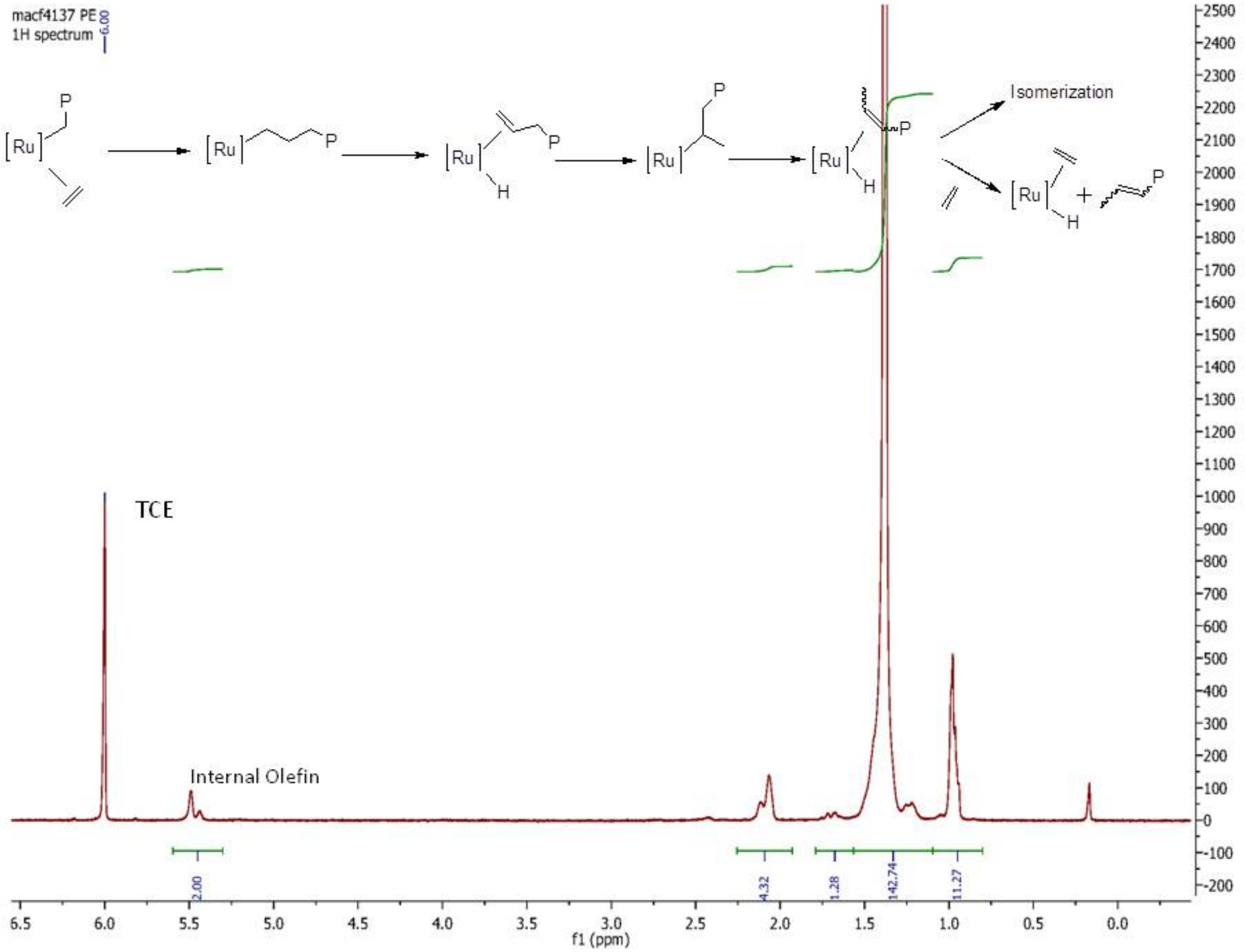

Figure S38. ^{1}H-NMR spectrum of polyethylene made by complex **4**/([H(Et$_2$O)$_2$]$^+$ [BAr'$_4$]$^-$).

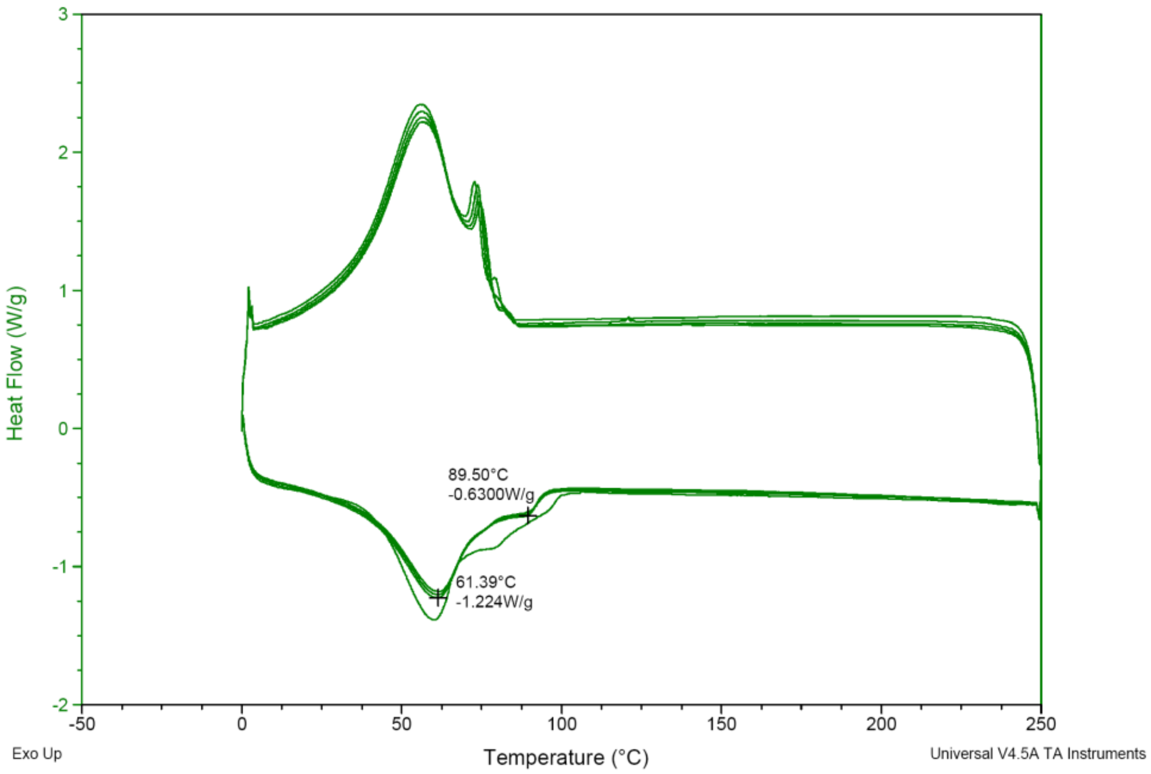

Figure S39. An example of DSC (table 1, entry 5) trace for polyethylene made by complex **4**/($[H(Et_2O)_2]^+$ $[BAr'_4]^-$).

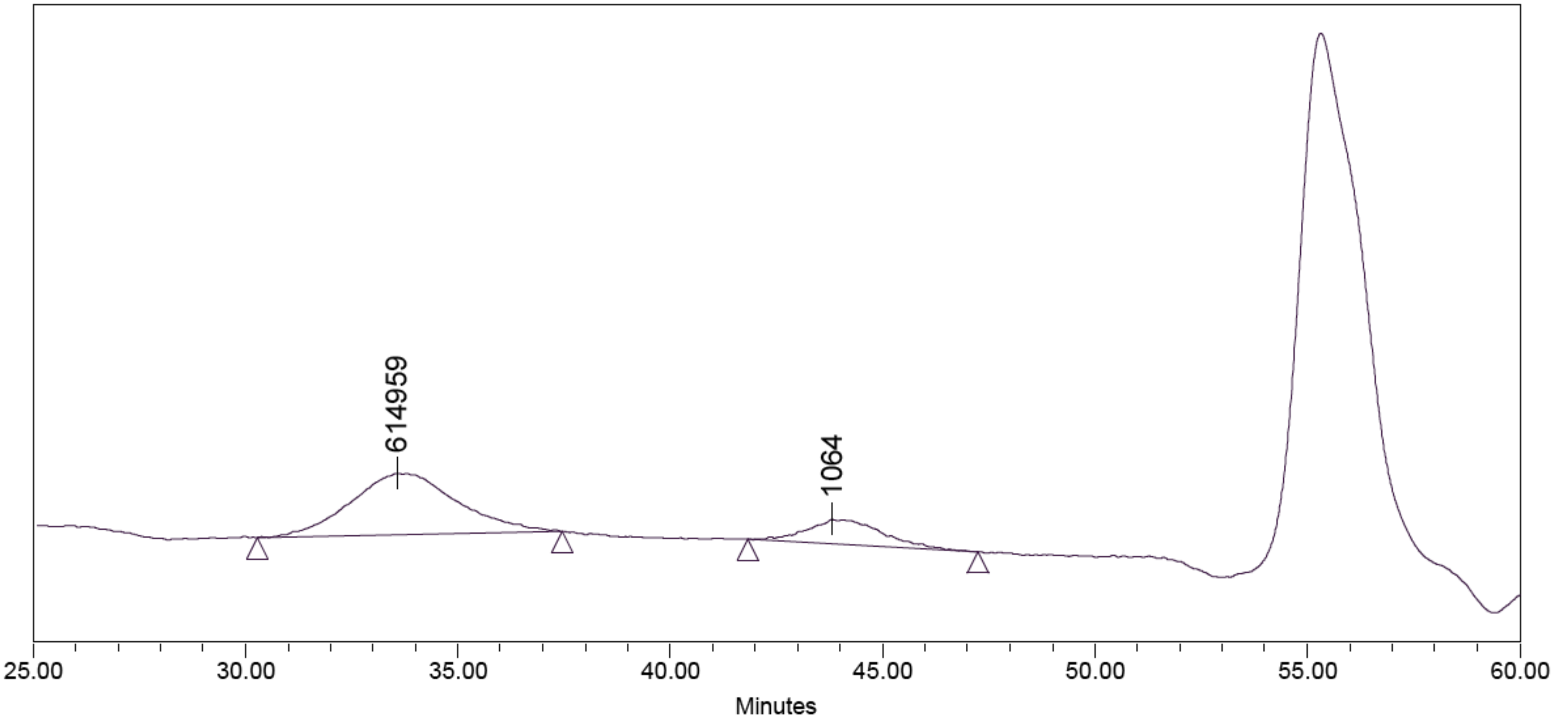

GPC Results

	Dist Name	Mn	Mw	MP	Mz	Mz+1	Mv	Polydispersity	MW Marker 1	MW Marker 2
1		262205	795002	614959	1797105	2694657		3.031991		
2		848	974	1064	1119	1278		1.148348		

Figure S40. An examples of GPC (table 1, entry 3) data for polyethylene made by complex **3**/Al Me_2Cl.

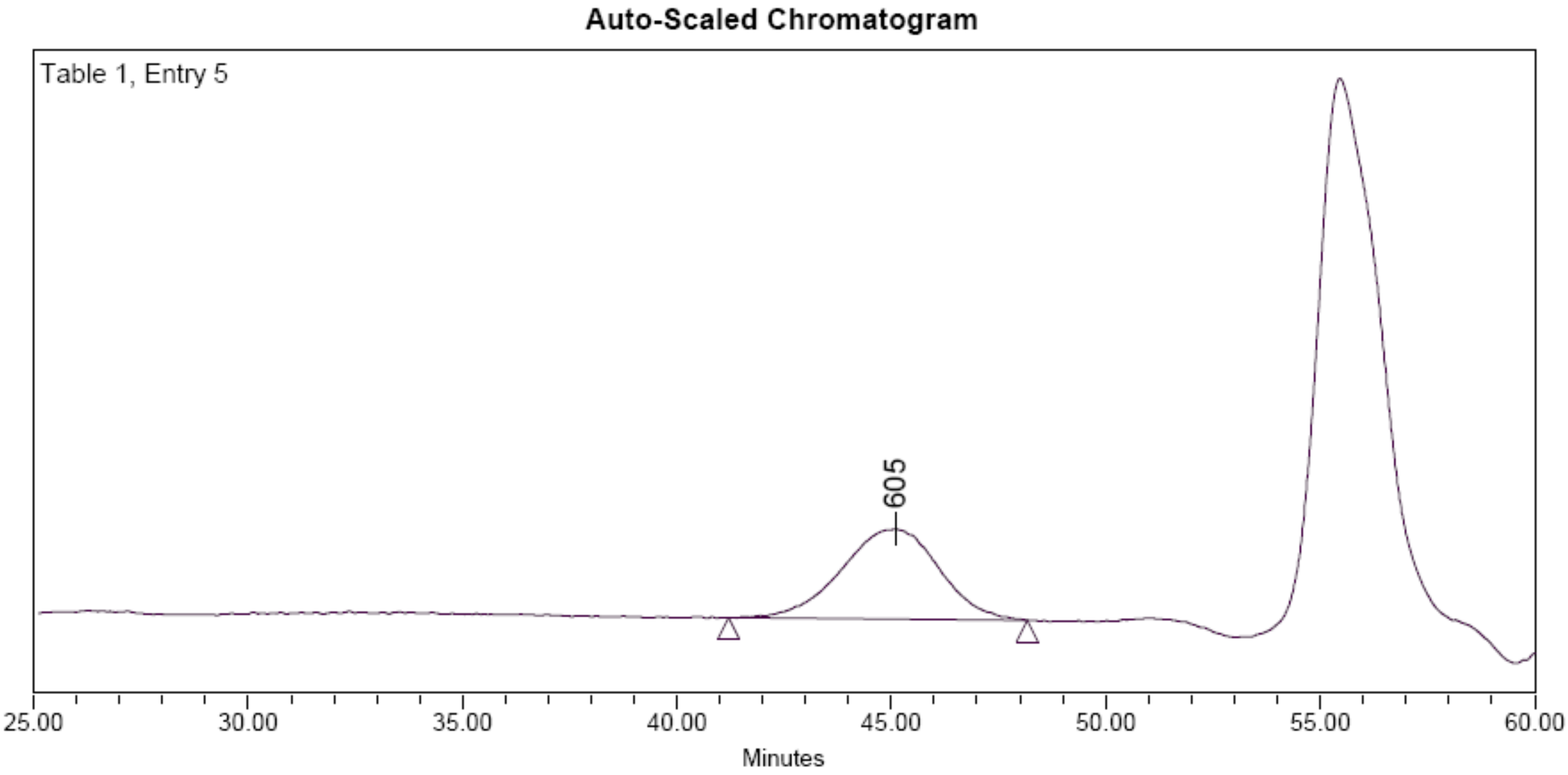

GPC Results

	Dist Name	Mn	Mw	MP	Mz	Mz+1	Mv	Polydispersity	MW Marker 1	MW Marker 2
1		610	724	605	890	1120		1.186637		

Figure S41. An examples of GPC (table 1, entry 5) data for polyethylene made by complex **4**/($[H(Et_2O)_2]^+$ $[BAr'_4]^-$).

References

1. M. Brookhart, B. Grant and A. F. Volpe Jr., *Organometallics*, 1992, **11**, 3920-3922.
2. O. Daugulis, M. Brookhart and P. S. White, *Organometallics*, 2002, **21**, 5935-5943
3. R. Ahlrichs, M. Bär, M. Häser, H. Horn and C. Kölmel, *Chem. Phys. Lett.*, 1989, **162**, 165-169.
4. N. E. Shevchenko, V. G. Nenajdenko and E. S. Balenkova, *Synthesis*, 2003, 1191-1200.
5. A. J. Birch, *J. Chem. Soc.*, 1944, 430-436.
6. O. Daugulis, M. Brookhart and P. S. White, *Organometallics*, 2003, **22**, 4699-4704.
7. APEX2 Version 2010.9-0, Bruker AXS, Inc.; Madison, WI 2010.
8. SAINT Version 7.68a, Bruker AXS, Inc.; Madison, WI 2009.
9. G. M. Sheldrick, SADABS, Version 2008/1, Bruker AXS, Inc.; Madison, WI 2008.
10. G. M. Sheldrick, SHELXTL, Version 2008/4, Bruker AXS, Inc.; Madison, WI 2008.
11. International Tables for X-Ray Crystallography 1992, Vol. C., Dordrecht: Kluwer Academic Publishers.
12. S. A. Svejda, L. K. Johnson and M. Brookhart, *J. Am. Chem. Soc.*, 1999, **121**, 10634-10635.